2019

OPTIMIZING NASAL CANNULAS FOR INFANTS USING COMPUTATIONAL FLUID DYNAMICS

Ahmad El-Achwah Mr.
Virginia Commonwealth University

OPTIMIZING NASAL CANNULAS FOR INFANTS USING COMPUTATIONAL FLUID DYNAMICS

A thesis submitted in partial fulfillment of the requirements for the Master of Science at Virginia Commonwealth University.

By

AHMAD BASSAM EL-ACHWAH

Bachelor of Science, Bridgewater College, USA, 2015

Director: Dr. P. WORTH LONGEST

Professor, Department of Mechanical and Nuclear Engineering and

Department of Pharmaceutics

Virginia Commonwealth University Richmond, Virginia

December, 2019

Acknowledgments

I would like to thank my advisor, Dr. Worth Longest, for giving me the opportunity to conduct meaningful research with a highly motivated group of scholars. Without his guidance and patience, I would not have been able to grow as an engineer. His mentorship has truly been invaluable This would also not be possible without the support and friendship of my lab-mates in the Longest Lab.

I am eternally grateful for the support and love that I have gotten from my mother, Hiam, my father, Bassam, and my two brothers Samir and Mahmoud in Lebanon. Without my parents sacrifices I would not be where I am today. To my dear wife, Nora Awadallah, who has been a major part of this journey with me, I am so thankful for having you by my side.

My committee members, Dr. James Miller and Dr. Thomas Roper, have been patient and supporting throughout this entire process. Dr. Karla Mossi, our graduate school department's program director, has given me the utmost support and guidance throughout this process and I am forever thankful for her role in the department.

Table of Contents

List of Figures 3
List of Acronyms 4
Abstract 5
Chapter 1: Background and Objectives 6
Chapter 2: Methods 13
Chapter 3 23
CFD validation using the particle reflection code 23
Effects of increasing flow rate 26
Effects of increasing wall roughness 28
Chapter 4 30
Streamlining the gradually expanding cannula 30
Modifying the stepped design 30
The co-flow design 32
Chapter 5 35
Optimizing the gradually expanding cannula 35
Optimizing the co-flow design 37
Chapter 6: Discussion and Conclusion 42

List of Figures

Figure 1: Gradual diffuser base design 13
Figure 2: Stepped diffuser base design 14
Figure 3: Initial gradual diffuser with co-flow design 14
Figure 4: WSS behavior in the gradual diffuser 23
Figure 5: WSS behavior in the stepped diffuser 24
Figure 6: Deposition fractions in the stepped diffuser using different WSS conditions 24
Figure 7: Gradual Diffuser DF as a function of WSS Threshold 25
Figure 8: Deposition fraction in the stepped diffuser as a function of WSS Threshold 25
Figure 9: DF in the gradual diffuser as a function of flow rate 26
Figure 10: Velocity field in the gradual diffuser at 2 L/min 26
Figure 11: Velocity field in the gradual diffuser at 3 L/min 26
Figure 12: Velocity field in the gradual diffuser at 4 L/min 27
Figure 13: Velocity field in the gradual diffuser at 5 L/min 27
Figure 14: Turbulent kinetic energy in the gradual diffuser at 2 L/min 27
Figure 15: Turbulent kinetic energy in the gradual diffuser at 3 L/min 27
Figure 16: Turbulent kinetic energy in the gradual diffuser at 4 L/min 27
Figure 17: Turbulent kinetic energy in the gradual diffuser at 5 L/min 28
Figure 18: Skin Friction Coefficient as a function of the gradual diffuser wall roughness 28
Figure 19: The effect of wall roughness and flow rate on aerosol losses 29
Figure 20: The effect of wall roughness and flow rate on aerosol loss without using the WSS code 29
Figure 21: Cumulative DF in the gradual Diffuser 31
Figure 22: Deposition fractions in various modifications of the stepped cannula 31
Figure 23: Flow field in stepped design, case 1..... 32
Figure 24: Flow field in a stepped design, case 2 32
Figure 25: Flow field in stepped design, case 3..... 32
Figure 26: Deposition fractions in the co-flow diffuser at 3 L/min 33
Figure 27: Deposition fractions in the co-flow diffuser at 5 L/min 33
Figure 28: Flow behavior in a co-flow design with 50 % central flow rate 34
Figure 29: Flow behavior in a co-flow design with 60 % central flow rate 34
Figure 30: Flow behavior in a co-flow design with 70 % central flow rate 34
Figure 31: Flow behavior in a co-flow design with 80 % central flow rate 34
Figure 32: Deposition fractions in four modified gradual diffuser designs at 3 and 5 L/min …. 34
Figure 33: Volume averaged flow variables in the four modified gradual diffuser designs at 3 and 5 L/min 36
Figure 34: Deposition fractions in the three modified co-flow cannulas at 3 and 5 L/min 37
Figure 35: Volume averaged flow variables in the three co-flow design variations 38
Figure 36: Deposition fraction in a 70 mm co-flow diffuser using various inlet velocity conditions at 3 L/min total flow rate 39
Figure 37: Deposition fraction in a 70 mm co-flow diffuser using various inlet velocity conditions at 5 L/min total flow rate 39
Figure 38: Turbulent kinetic energy contours in a 70 mm co-flow cannula midplane when a) V1/V2=2.34, b) V1/V2= 1.7, and c) V1/V2=0.7. 40
Figure 39: Particle deposition maps in a 70 mm co-flow cannula when a) V1/V2=2.34, b) V1/V2= 1.7, and c) V1/V2=0.7 41

List of Acronyms

CFD	Computational Fluid Dynamics
DF	Deposition Fraction
DPI	Dry Powder Inhaler
EEG	Expedient Enhanced Growth
LRN	Low-Reynolds Number
MMAD	Mass median aerodynamic diameters
PSD	Particle Size Distribution
C_f	Skin Friction Coefficient
TKE	Turbulent Kinetic Energy
UDF	User Defined Functions
WSS	Wall Shear Stress
WSS_{max}	Wall Shear Stress maximum value

Abstract

Aerosolized medications can potentially be delivered to the lungs of infants through a nasal cannula interface. However, nose-to-lung delivery technologies currently allow for ~1% of the loaded dose to reach an infant's lungs. Conventional dry powder inhalers (DPI) are superior to other types of inhalers in many ways. However, passive DPIs that operate based on user inhalation and require large volumes of airflow are not applicable to infants. To overcome this challenge, positive pressure DPIs have been developed that enable aerosol delivery to infants. Unless an adequate nasal interface is used with these devices, a significant amount of drug will still be lost. Computational fluid dynamics (CFD) provide a method to assess the performance of a nasal cannula interface and optimize its performance. In this study, a CFD model was first experimentally validated using the low-Reynolds number k-ω turbulence model, then used to assess and optimize several conical diffuser cannula designs for infants. The performance of a cannula depends primarily on two requirements: the amount deposited particles and the cannula's volume. It was found that 90 and 100 mm long simple diffusers achieved the necessary deposition and volume requirements when operated at 3 and 5 liters per minute, respectively. Additionally, including clean sheath co-flow air with the 70 mm long diffuser achieved the targeted performance requirements. Inclusion of recent advancements in the field with the recommended cannula designs is likely to improve pharmaceutical aerosol delivery to infants using the nose-to-lung approach.

Chapter 1: Background and Objectives

The delivery of pharmaceutical aerosols to the lungs provides an effective method to treat many respiratory diseases and conditions (1). Considering infants, aerosolized surfactant therapy, antibiotics, corticosteroids, and anti-inflammatory medications are all envisioned future remedies (2-4). Advantages of the aerosolized approach include increased dose delivered to the site of action. This targeted approach leads to increased efficacy of the medication, and reduced side effects associated with offsite dosage. However, aerosol administration to infants has only been realized for one or two medications with low dosages and mild side effects, due to very poor lung delivery efficiency (5-7). Using current aerosol delivery technologies, only ~ 1% of a dose loaded into an inhaler or nebulizer reaches an infant's lungs (6-9). Moreover, this dose is typically deposited in the upper tracheobronchial region, which is often not the intended target. In order to make most envisioned inhaled medications a reality in infants, lung delivery efficiency should be dramatically improved.

Dry powder inhalers (DPI) provide a convenient platform for respiratory drug delivery with many advantages including rapid administration, stable formulations, and the ability to deliver high doses of medications compared with metered dose inhalers and nebulizers (10). Primary disadvantages of DPIs include: the need for large air volumes to aerosolized the powder, on the order of 4 L, high device retention of drug, and high depositional loss of aerosol in the delivery system and subject extrathoracic airways (11). All commercial DPIs are also passive devices requiring the subject to actively inhale through the device with a pressure drop of at least 1.6 kPa and typically 4 kPa, which is not possible for infants. Some of these disadvantages can be mitigated through the use of active devices that incorporate a positive pressure gas source to generate the aerosol. At VCU, our group has developed active DPI devices that can generate an

aerosol with air volumes as small as 3 to 10 ml (12-15). These devices work on an air-jet principle (16, 17) that combines a small diameter air inlet, aerosol chamber and small diameter aerosol outlet. Positive pressure air is passed through the small diameter inlet capillary into the aerosolization chamber forming a high speed turbulent and compressible air jet. This air jet initially fluidizes the powder and then further deaggregates the powder through turbulence. The aerosol is then transported out through the outlet capillary. Excellent aerosolization is achieved with this arrangement using emitted doses on the order of 80% of loaded dose and aerosol mass median aerodynamic diameters (MMADs) of approximately 1.5 μm (16, 17). However, a primary disadvantage of this approach is the formation of a high-speed air jet that may result in excess aerosol loss unless it is sufficiently dispersed. Dissipation of a high-speed jet of air containing particles in a confined space without excessive depositional aerosol loss is a significant challenge.

In a DPI, the patient interface is the region between the aerosol generation unit and the subject. For the air jet DPI, the interface spans the region between the aerosolization chamber outlet capillary and subject's nose or mouth. For infants, this patient interface region is intended to be a nasal cannula between the outlet capillary and one or both infant nostrils. In the infant air-jet DPI, this nasal cannula is required to dissipate the turbulent jet while minimizing depositional losses in the cannula and in the infants extrathoracic airways. Moreover, envisioned air volumes to preterm and term neonates are expected to be approximately 10 ml and 30 ml, respectively. The interface should therefore have a maximum volume on the order of 1 ml, to minimize the amount of aerosol lost to dead volume, i.e, not deposited but left in the air at the end of aerosol delivery.

The **goal** of this study is to develop a validated CFD model and then use this model to explore and optimize multiple cannula designs for high efficiency aerosol delivery to infants from an air-jet DPI. Potential cannula designs to be considered in this work include a gradual diffuser, stepped diffuser, and co-flow air approach. Cannula volume should remain below 10% of the air used to generate the aerosol. Expected gas flow rates are in the range of 2 to 5 L/min. Depositional losses should be below 5% total. Conditions for single configuration cannulas are evaluated in this study for full term infants. Successful designs will achieve the desired metrics and introduce the least amount of complexity into the system. Objectives to accomplish this overarching goal are outlined below.

Objective 1: Develop a validated CFD model of aerosol deposition in the infant nasal cannula system compared with *in-vitro* experimental results employing an air-jet DPI.

Rationale. The infant cannula system appears simple but is deceptively complex. The base case is a smooth expansion from 0.89 mm to 4 mm over a length of 63 mm. Both turbulent and a transition to laminar flow are expected to occur. Surface wall roughness will influence this transition. Furthermore, surface wall roughness and laminar vs. turbulent flow strongly affect boundary layer detachment from the surface. When boundary layer detachment occurs, depositional loss will dramatically increase in the region of recirculation and reattachment. Wall shear stress (WSS) may also play a role in deposition with high WSS values leading to surface detachment of particles.

Methods. Based on previous successful simulations with aerosol deposition in turbulent and transitional flows, the low Reynolds number (LRN) k-ω turbulence model will be employed (18, 19). The commercial CFD package Fluent 19 is used as a base platform for solving the

equations of motion. Available sub-models for wall surface roughness are implemented. User routines to account for a threshold WSS above which particles do not deposit are developed. Due to the straightforward geometry, a hexahedral mesh scheme with high accuracy will be employed.

Outcomes. Successful validation of the CFD model will be achieved when deposition predictions for a polydisperse aerosol are within 10% relative difference of the experimental data under steady state flow conditions. Validations will be sought for the gradual and stepped diffuser designs.

Objective 2. Conduct a parametric sensitivity analysis of key features related to each design.

Rationale. Key features regarding each design type will be considered. For the gradual diffuser, the design will be streamlined to avoid particle loss upon sharp turns. Considering the stepped diffuser, the length of each step will be reduced while the total length of the cannula will be maintained. Modifying the step length could affect boundary layer de-attachment, consequently, this will affect aerosol deposition. Allowing a sheath airflow around the central jet of a gradual diffuser will affect deposition fractions depending on the flow rate distribution between the central and the external inlets.

Methods. Similar routines in meshing, CFD case set up, and particle injection from Objective 1 are repeated. Streamlining the gradual diffuser was done by smoothing sharp angles at the inlet and outlet of the cannula. For the stepped diffuser three different variations in step length were utilized. For the co-flow gradual diffuser, four different distributions between central and external flow rates were applied.

Outcome. Streamlining the gradual diffuser only reduced deposition fraction by 1%. Reducing the length of the step in the stepped diffuser lead to an increase deposition fraction. Assigning the external flow rate of the co-flow diffuser below 50 % of the total flow rate increased deposition fraction.

Objective 3. Study the effects of lengthening both types of gradual diffusers and modify the inlet boundary conditions for the co-flow design.

Rational. Modifying the size of the cannula could have a significant effect on the onset of boundary layer de-attachment as well as the amount of turbulent kinetic energy present in the system. For the co-flow diffuser, adjusting inlets boundary conditions based on their relative velocity ratios can alter certain flow properties that would affect particle deposition.

Methods. Similar routines in meshing, CFD case set up, and particle injection from Objective 1 are repeated

Outcome. Wall shear stress and turbulent kinetic energy were the primary factors affecting nasal cannula particle deposition. Ninety mm and 100 mm gradually expanding cannulas were predicted to achieve targeted delivery conditions at 3 L/min, and 5 L/min, respectively. A 70 mm co-flow cannula also achieved the desired conditions by providing the required sheath airflow around the central jet.

References

1. Patton JS, and Byron PR. Inhaling medicines: delivering drugs to the body through the lungs. *Nature Reviews Drug Discovery.* 2007;6:67-74.

2. Rubin BK. Pediatric aerosol therapy: New devices and new drugs. *Respiratory Care.* 2011;56:1411-1421.

3. Rubin BK, and Fink JB. Novel medications for asthma: a look at the future. *Expert Opinion on Investigational Drugs.* 2007;16:889-897.

4. Rubin BK, and Williams RW. Emerging aerosol drug delivery strategies: from bench to clinic. *Advanced Drug Delivery Reviews.* 2014;75:141-148.

5. Rubin BK, and Fink JB. Aerosol therapy for children. *Respir Care Clin N Am.* 2001;7:175-213.

6. Fink JB. Aerosol delivery to ventilated infant and pediatric patients. *Respiratory Care.* 2004;49:653-665.

7. Fink JB. Delivery of inhaled drugs for infants and small children: a commentary on present and future needs. *Clinical Therapeutics.* 2012;34:S36-S45.

8. Sunbul FS, Fink JB, Harwood R, Sheard MM, Zimmerman RD, and Ari A. Comparison of HFNC, bubble CPAP and SiPAP on aerosol delivery in neonates: An in-vitro study. *Pediatric Pulmonology.* 2015;50:1099-1106.

9. El Taoum KK, Xi J, Kim J, and Berlinski A. In vitro evaluation of aerosols delivered via the nasal route. *Respiratory Care.* 2015;60:1015-1025.

10. Islam N, and Cleary MJ. Developing an efficient and reliable dry powder inhaler for pulmonary drug delivery - A review for multidisciplinary researchers. *Medical Engineering and Physics.* 2012;34:409-427.

11. Newman SP, and Busse WW. Evolution of dry powder inhaler design, formulation, and performance. *Respiratory Medicine.* 2002;96:293-304.

12. Farkas D, Hindle M, Bonasera S, Bass K, and Longest W. Development of an inline dry powder inhaler for oral or trans-nasal aerosol administration to children. *Journal of Aerosol Medicine and Pulmonary Drug Delivery.* 2019;DOI: 10.1089/jamp.2019.1540

13. Farkas D, Hindle M, and Longest PW. Development of an inline dry powder inhaler that requires low air volume. *Journal of Aerosol Medicine and Pulmonary Drug Delivery.* 2018;31:255-265.

14. Farkas D, Hindle M, and Longest PW. Application of an inline dry powder inhaler to deliver high dose pharmaceutical aerosols during low flow nasal cannula therapy. *International Journal of Pharmaceutics.* 2018;546:1-9.

15. Farkas D, Hindle M, and Longest PW. Efficient Nose-to-Lung Aerosol Delivery with an Inline DPI Requiring Low Actuation Air Volume. *Pharmaceutical Research.* 2018;35:194.

16. Longest W, and Farkas D. Development of a New Inhaler for High-Efficiency Dispersion of Spray-Dried Powders Using Computational Fluid Dynamics (CFD) Modeling. *The AAPS Journal.* 2019;21:25.

17. Longest W, Farkas D, Bass K, and Hindle M. Use of Computational Fluid Dynamics (CFD) Dispersion Parameters in the Development of a New DPI Actuated with Low Air Volumes. *Pharmaceutical Research.* 2019;36:110.

18. Longest PW, Bass K, Dutta R, Rani V, Thomas ML, El-Achwah A, and Hindle M. Use of computational fluid dynamics deposition modeling in respiratory drug delivery. *Expert Opin. Drug Deliv.* 2019;16:7-26.

19. Longest PW, and Holbrook LT. In silico models of aerosol delivery to the respiratory tract - Development and applications. *Advanced Drug Delivery Reviews.* 2012;64:296-311.

Chapter 2: Methods

Base Cannula Designs

An aerosol is formed in an air-jet DPI with an outlet diameter of 0.89 mm. These devices are intended to diffuse the high velocity jet of air with minimal particle depositional loss. The air jet enters the left-hand side of the cannula (Figure (1)) while the right-hand side is connected to the infant nostrils. The most basic approach to diffuse the air jet is through a gradually expanding diffuser as shown in Figure (1). The angle of the diffuser should be adjusted such that wall separation of the boundary layer does not occur.

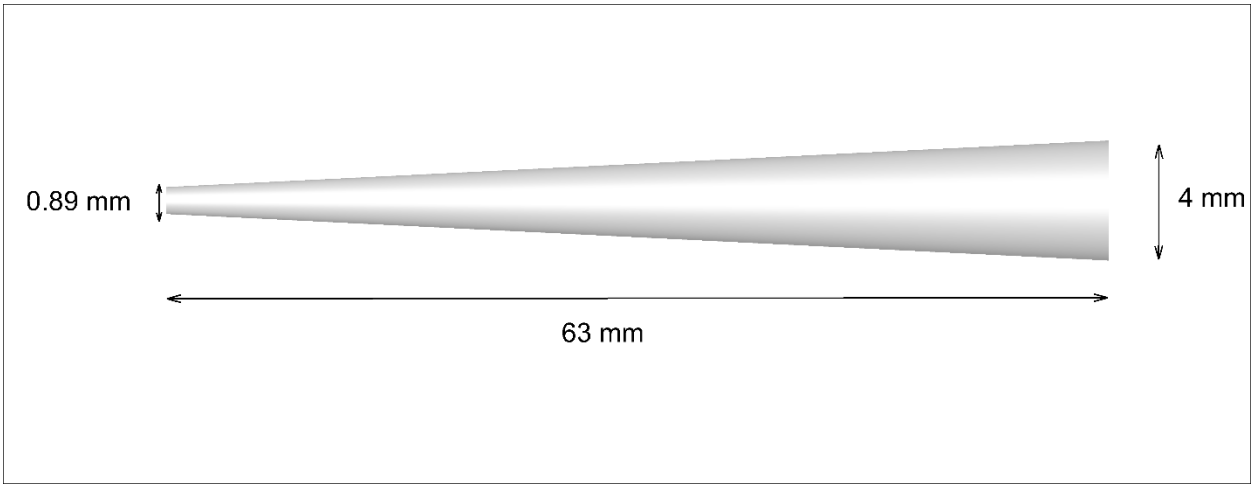

Figure 1: Gradual diffuser base design

A disadvantage of this approach is the unfamiliarity with the length and volume required to ensure that separation of boundary layer does not occur. A possible improvement of this design can be done by reducing the length of the diffuser enough to avoid boundary layer de-attachment. However, since the diffuser outlet size is based on a fixed nostril diameter of 3-4 mm for preterm and full-term infants, respectively, a stepped-style diffuser can be implemented as shown in Figure (2).

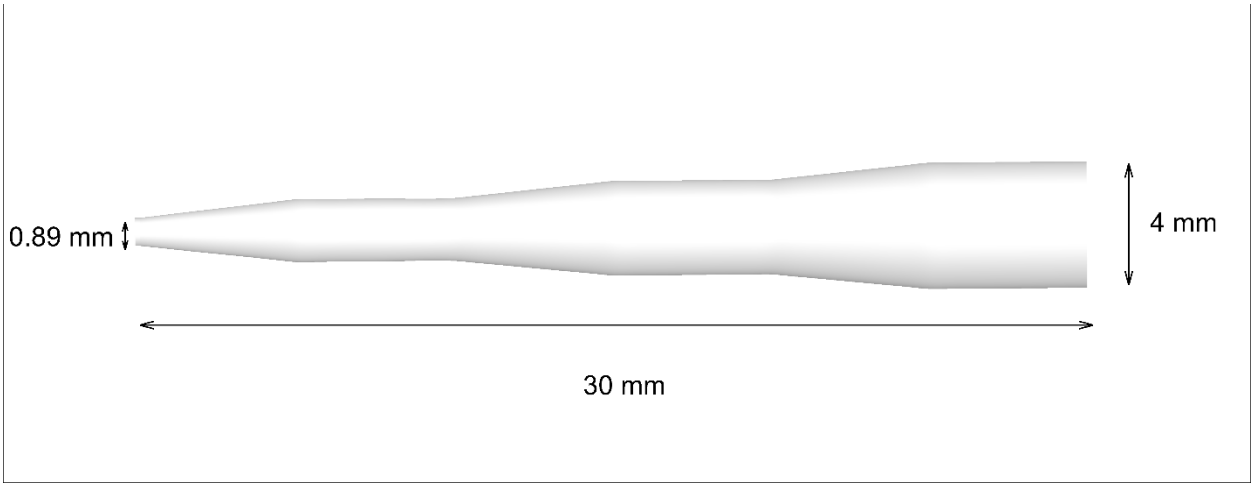

Figure 2: Stepped diffuser base design.

A subtype of gradual diffuser will have a 1 mm larger inlet diameter than the previously implemented diffuser (Figure 3). This extra area will allow a sheath airflow around the central jet at the specified flow rate.

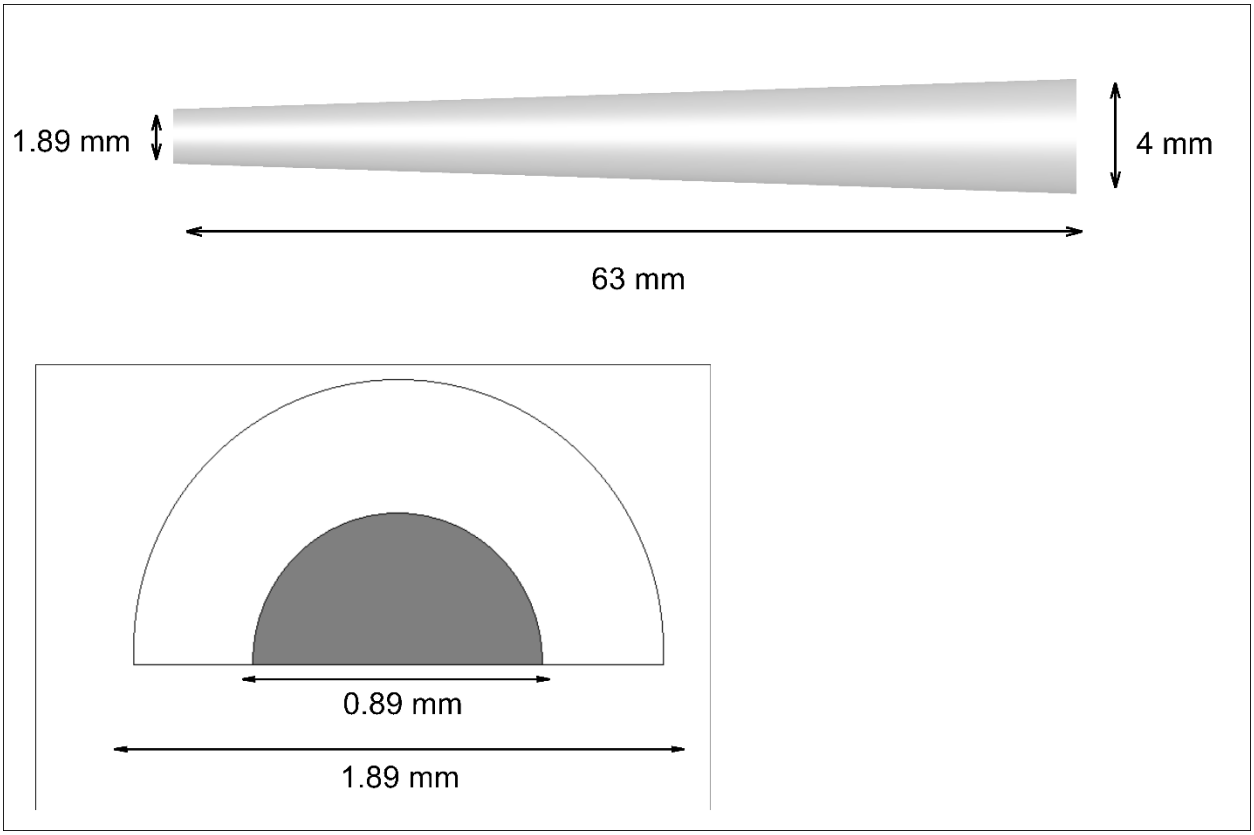

Figure 3: Initial gradual diffuser with co-flow design. Both central (filled region) and external (empty region) cannula inlets are shown as well.

Mesh Generation

Recommendations on grid generation and flow simulation setup were based on our previous studies [1] [2] [3]. All grids were constructed with high quality hexahedral cells using GAMBIT 2.4.6 (ANSYS Inc., Canonsburg, PA). Grid independent results were achieved with mesh sizes ranging from 660,000 to 880,000 cells depending on the geometry size. Increased mesh density was necessary near the walls. Negligible changes (< 3 %) in volume averaged velocity and turbulent kinetic energy values were major criteria in mesh density choice.

CFD Setup

Flow rates ranging between 2-5 L/min are associated with inlet Reynolds numbers ranging between 3228 and 8072. Thus, transitional and turbulent flows are expected to occur as air passes through cannula.

The CFD package Fluent 19 (ANSYS Inc., Canonsburg, PA) was utilized to solve governing equations of mass and momentum, and particle trajectory. Pressure-based solver and SIMPLEC pressure coupling were implemented under steady state-assumptions. Based on previous studies [1, 4, 5], the two-equation low Reynolds number (LRN) k-ω model with shear flow corrections was the most appropriate turbulence model in this study. This model provides a balance between accuracy in predicting particle deposition and numerical efficiency. Equations governing this model can be found in prior publications [6, 7]. Transport equations were discretized to be at least second order accurate in space.

A user-created Fortran code allowed the generation of a polydisperse inlet particle profile. Experimentally determined particles size distribution (PSD) was used *in-silico* to inject particles as well as calculate their deposition fractions in different regions of the cannula designs.

Eight bins of different sizes with 5000 particles per bin were used to represent the PSD. Particles were assumed to be spherical water droplets with density of 1.0 g/cm^3. In simulations that compared with experimental validations, the estimated density of the particle was used to form the correct aerodynamic diameter. Injecting beyond 5000 particles per bin had negligible effect on deposition fractions. Lagrangian particle tracking algorithm was implemented to determine particles fates. Random Walk was activated to account for the random effects of turbulence on particle dispersion. In addition to turbulent dispersion, drag and gravity effects were assumed to be the forces acting on each particle. Equations governing particle tracking can be found in references [8, 9].

Wall Surface Sub-model

In a previous study by our group, CFD validations of *in-vitro* aerosol deposition in airway models were achieved using wall roughness-based simulations [10]. While these results were not sensitive to certain levels of wall roughness considered, this was attributed to the laminar flow nature used in this study. However, the effect of surface roughness was anticipated to become more significant as flow rate is increased and turbulent eddies became stronger. In this study, both transitional and turbulent flow regimes are present. The wall roughness sub-model is implemented for two purposes: first, to experimentally validate our CFD model, and, second, to explore the effects of wall roughness in different flow regimes.

In turbulent regimes, the law-of-the-wall is modified by a downward shift of the logarithmic non-dimensional velocity profile, u^*, by some ΔB value shown in the Equation (1)**:**

$$\frac{u_p u^*}{\tau_w/\rho} = \frac{1}{\kappa}\ln\left[\mathrm{E}\frac{\rho u^* y_p}{\mu}\right] - \Delta\mathrm{B} \quad (1)$$

where $u^* = C_\mu^{1/4}\kappa^{1/2}$ is a dimensionless velocity,

κ is Von-Karman Constant,

C_μ is an empirical constant

u_p is the mean velocity of the fluid at a near wall node p,

E is an empirical constant,

ρ is the density of the fluid,

τ_w is the wall shear stress,

μ is the dynamic viscosity of air,

and y_p is the distance from point p to the wall.

However, Shifting the u^* values by ΔB excludes any wall treatment for large roughness heights and low values of y^+. To solve this problem, Fluent follows a "virtual wall shift" approach, which will not be discussed in this work but can be found in The Fluent Theory Guide [11].

ΔB is known to be directly related to an arbitrary roughness function f_r : $\Delta B = \frac{1}{\kappa} ln f_r$. However, there is no universal roughness function valid for all types of roughness. Under the sand-grain roughness assumption, a non-dimensional roughness height $K_s^+ = \rho K_s u^*/\mu$ was found to correlate well [12] with ΔB depending on the K_s^+ values:

Under no roughness effects, $K_s^+ \leq 2.25$, the law-of-the-wall is unchanged. i.e:

$$\Delta\mathrm{B} = 0 \quad (2)$$

For transitional regime, $2.25 < K_s^+ \leq 90$:

$$\Delta B = \frac{1}{\kappa} \ln \left[\frac{K_s^+}{87.75} + C_s K_s^+ \right] \times \sin\{0.4258(\ln K_s^+ - 0.8111)\} \quad (3)$$

and for a fully rough regime, $K_s^+ \geq 90$:

$$\Delta B = \frac{1}{\kappa} \ln(1 + C_s K_s^+). \quad (4)$$

where C_s is a roughness constant.

In Fluent 19, the uniform sand-grain roughness model is activated by specifying two variables: the roughness height, K_s, and roughness constant, C_s. In this study, several roughness heights were considered. However, no clear guidance on the choice of C_s is available. For k-ε turbulence model, The Fluent User Guide recommends using C_s=0.5 for pipe flows. The same value is used in this study.

WSS-Based Particle Reflection UDF

In-vitro investigation of powder losses in the expanding diffuser revealed that the majority of the deposit losses occur far from the cannula inlet. However, initial attempts to validate these findings resulted in an overestimation of powder loss near inlet and, consequently, an over-prediction of the total deposition losses in the cannula.

These observations suggested that shear stress arising from the airflow in small diameter regions may strip of deposited particles. A user-created C code was incorporated in our CFD model to for two purposes: first, to correctly predict shear stress behavior on the cannula surface and, then, to decide the fate of each particle upon wall impact.

In the first step of the program, the code loops through each face of the cannula boundary, calculates the velocity gradient at its centroid, and multiplies it by the effective viscosity,($\mu + \mu_T$), of the first neighboring cell. i.e:

$$\tau_w = (\mu + \mu_T)\frac{\Delta u_t}{\Delta y}. \quad (5)$$

In this equation, Δy is the distance between the centroid of a boundary face and its first neighboring cell. Δu_t is the tangential velocity component of a face-neighboring cell, which is computed by subtracting the normal velocity component from the total velocity in each face-neighboring cell. i.e:

$$\Delta u_t = |u| - \vec{u} \bullet \overrightarrow{F_A} \quad (6)$$

where $\overrightarrow{F_A}$ is a face-unit normal vector.

The eddy viscosity term, μ_t, is calculated according to the equations provided in Fluent User Guide which are replicated here:

$$\mu_t = \alpha^* \frac{\rho k}{\omega} \quad (7)$$

where k and ω are the turbulence kinetic energy and the specific rate of dissipation, respectively. The equation for μ_t includes a damping coefficient, α^*,that allows for a low-Reynolds number correction. This damping coefficient is a function of fluid constants and transport variables, as follows:

$$\alpha^* = \alpha_\infty^* \left[\frac{\alpha_0^* + {Re_t}/{R_k}}{1 + {Re_t}/{R_k}}\right] \quad (8)$$

$$Re_t = \frac{\rho k}{\mu_{Lam} w} \quad (9)$$

where $R_k = 6$, $\beta_i = 0.0072$,and $\alpha_0^* = \frac{\beta_i}{3}$.

A more thorough explanation of Equations (7-9) can be found in most turbulence modeling textbooks, for example: [5].

The second part of the program is a WSS-based condition for particles to reflect after surface impact. The user defines WSS threshold at which this reflection is allowed to occur. An example from Fluent UDF Manual was used predict the velocity vectors of reflected particles. The equation governing particle reflection upon surface impact can be stated as:

$$\vec{V_p'} = \vec{V_p} - 2\left(\overrightarrow{V_p}.\overrightarrow{F_A}\right)\overrightarrow{F_A} \qquad (10)$$

where $\vec{V_p}$ and $\vec{V_p'}$ are the velocity vectors for incident and reflected particles, respectively. Normal and tangential coefficients of restitution are set to one and are, thus, omitted from Equation (10) for simplicity.

References

1. Bass, K. and P.W. Longest, *Recommendations for simulating microparticle deposition at conditions similar to the upper airways with two-equation turbulence models.* Journal of Aerosol Science, 2018. **https://doi.org/10.1016/j.jaerosci.2018.02.007**.

2. Vinchurkar, S. and P.W. Longest, *Evaluation of hexahedral, prismatic and hybrid mesh styles for simulating respiratory aerosol dynamics.* Computers and Fluids, 2008. **37**(3): p. 317-331.

3. Longest, P.W. and L.T. Holbrook, *In silico models of aerosol delivery to the respiratory tract - Development and applications.* Advanced Drug Delivery Reviews, 2012. **64**: p. 296-311.

4. Longest, P.W., et al., *Aerodynamic factors responsible for the deaggregation of carrier-free drug powders to form micrometer and submicrometer aerosols.* Pharmaceutical Research, 2013. **30**: p. 1608-1627.

5. Wilcox, D.C., *Turbulence Modeling for CFD, 2nd Ed.* 1998, California: DCW Industries, Inc.

6. Longest, P.W., et al., *Numerical simulations of capillary aerosol generation: CFD model development and comparisons with experimental data.* Aerosol Science and Technology, 2007. **41**(10): p. 952-973.

7. Longest, P.W., S. Vinchurkar, and T.B. Martonen, *Transport and deposition of respiratory aerosols in models of childhood asthma.* Journal of Aerosol Science, 2006. **37**: p. 1234-1257.

8. Longest, P.W. and J. Xi, *Effectiveness of direct Lagrangian tracking models for simulating nanoparticle deposition in the upper airways.* Aerosol Science and Technology, 2007. **41**(4): p. 380-397.

9. Longest, P.W., et al., *Comparison of ambient and spray aerosol deposition in a standard induction port and more realistic mouth-throat geometry.* Journal of Aerosol Science, 2008. **39**(7): p. 572-591.

10. Holbrook, L.T. and P.W. Longest, *Validating CFD predictions of highly localized aerosol deposition in airway models: In vitro data and effects of surface properties.* Journal of Aerosol Science, 2013. **59**: p. 6-21.

11. Fluent, A., *18.2, Theory Guide, ANSYS Inc.* Canonsburg, PA, 2017.

12. Cebeci, T. and P. Bradshaw, *Momentum transfer in boundary layers, Hemisphere Publ.* Corp., Washington-London, 1977.

13. Longest, P.W., L. Golshahi, and M. Hindle, *Improving pharmaceutical aerosol delivery during noninvasive ventilation: Effects of streamlined components.* Annals of Biomedical Engineering, 2013. **41**(6): p. 1217-1232.

14. Golshahi, L., et al., *The use of condensational growth methods for efficient drug delivery to the lungs during noninvasive ventilation high flow therapy.* Pharmaceutical Research, 2013. **30**: p. 2917-2930.

15. White, F.M., *Fluid mechanics.* 2015.

16. Fox, R.W. and S. Kline, *Flow regimes in curved subsonic diffusers.* Journal of Basic Engineering, 1962. **84**(3): p. 303-312.

17. Moore Jr, C.A. and S.J. Kline, *Some effects of vanes and of turbulence in two-dimensional wide-angle subsonic diffusers.* 1958.

18. McDonald, A.T. and R.W. Fox, *Incompressible Flow in Conical Diffusers*. 1964, PURDUE RESEARCH FOUNDATION LAFAYETTE IN LAFAYETTE United States.

Chapter 3

CFD validation using the particle reflection code

In vitro experiments revealed that deposited particles were being stripped off from both stepped and gradual cannulas due to high shear stress near the capillary inlet. Experimental DFs were 19.5 % and 13.2 % for the stepped and gradual diffusers, respectively. Standard deviations were around 2.5 % for both designs. For the stepped diffuser, only 1 % of the total powder loss was found to occur within the first 5 mm.

Since initial CFD runs were unable to capture these observations, it was established that our model needs to be adjusted in order to match the *in-vitro* experimental deposition data. Based on Equations (5-10), a program written in C language was designed to account for the influence of WSS on particle deposition. WSS profiles for both diffusers are shown in Figures (4) and (5). While there are large variations in the WSS behavior between the two designs, designating a critical WSS value above which particle reflection starts can improve both validation and optimizations stages of the study.

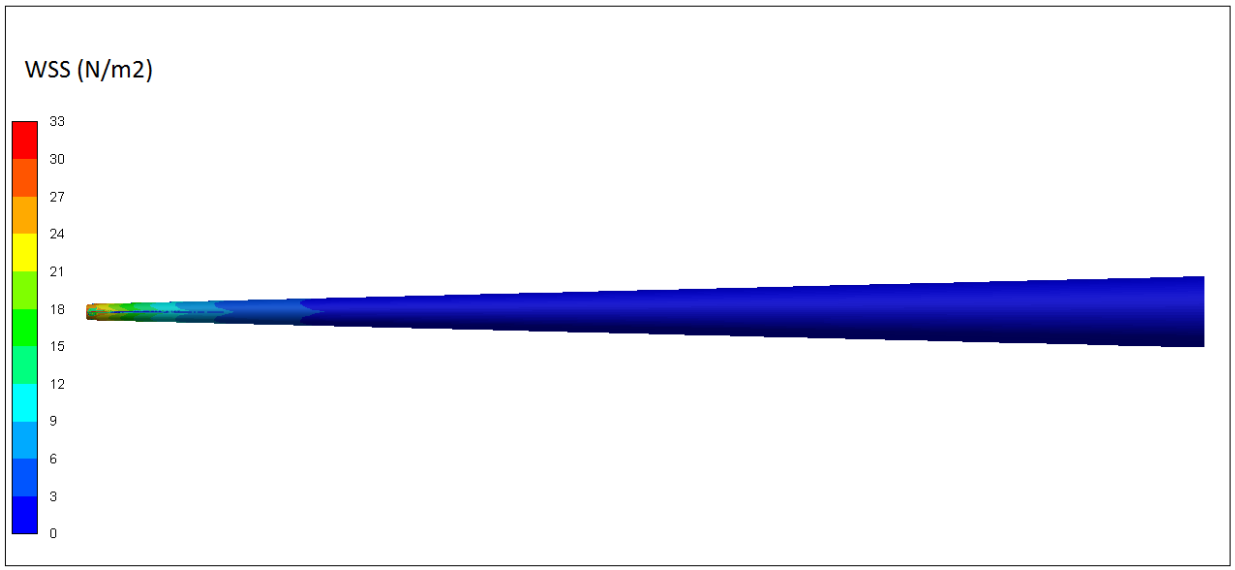

Figure 4: WSS behavior in the gradual diffuser

Figures (5) and (6) of the stepped diffusers show that WSS provides an explanation for particle deposition as an additional mechanism. Particles will deposit if the shear stress on the surface of is smaller than the defined limit and will reflect if the shear stress is greater than the defined limit.

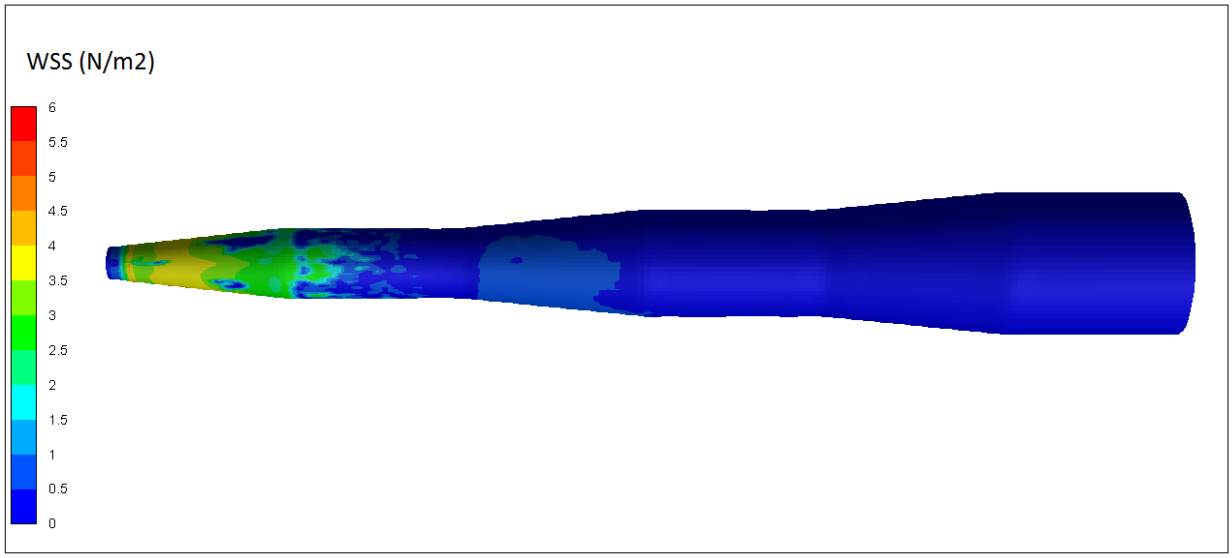

Figure 5: WSS behavior in the stepped diffuser

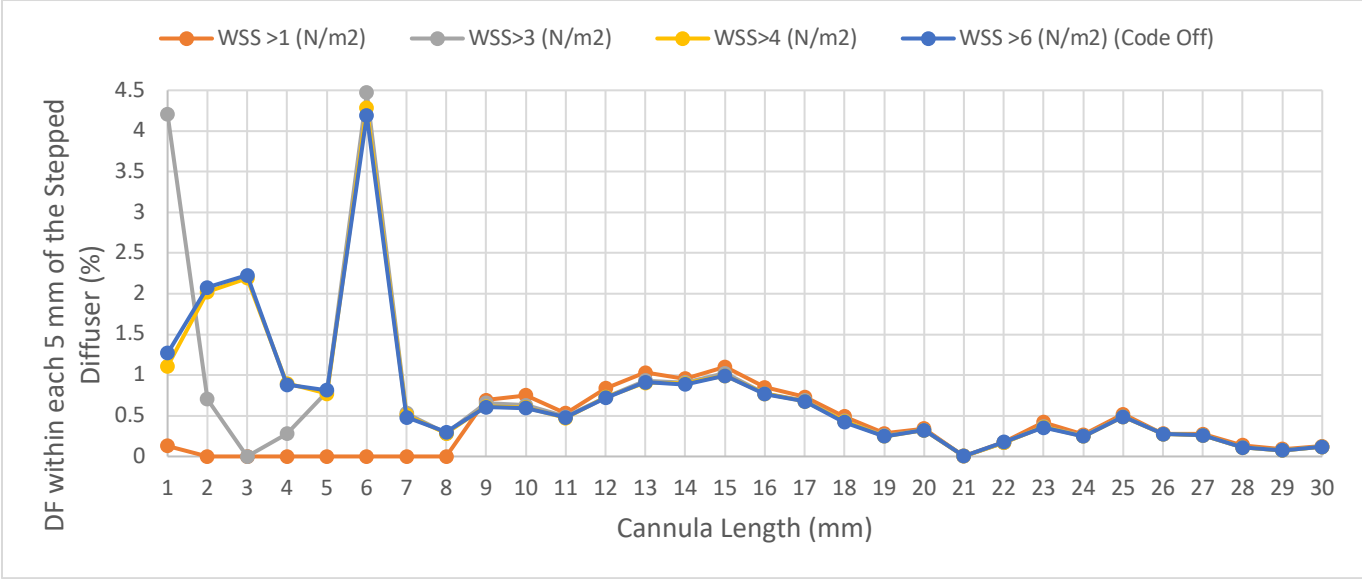

Figure 6: Deposition fractions in the stepped diffuser using different WSS conditions.

Figures (7) and (8) show the variation of total DF as a function of the WSS limit value condition. Setting a WSS threshold between 3 and 9 N/m^2 closely approximates experimental DF in the

gradual diffuser. Setting this threshold between 1.7 and 4 N/m^2 provides a close prediction to the experimental DF in the stepped diffuser. Thus, a mutual WSS threshold ranges between 3 and 4 N/m^2 to address both cases. For the rest of the study, WSS critical value =3 N/m^2 will be used as a default particle reflection condition. Using this condition, our CFD predictions fall within one standard deviation of the experiments for both designs. While this condition overpredicts DF in the first 5 mm step of the stepped diffuser by a few percent, it still outperforms the rest of the conditions in predicting aerosol losses within this region.

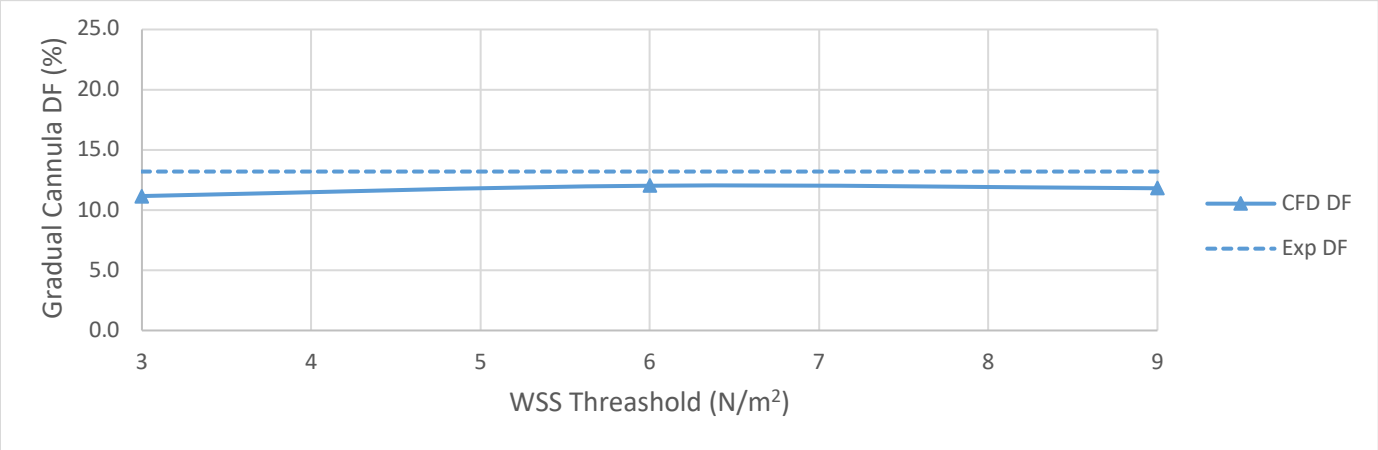

Figure 7: Gradual Diffuser DF as a function of WSS Threshold

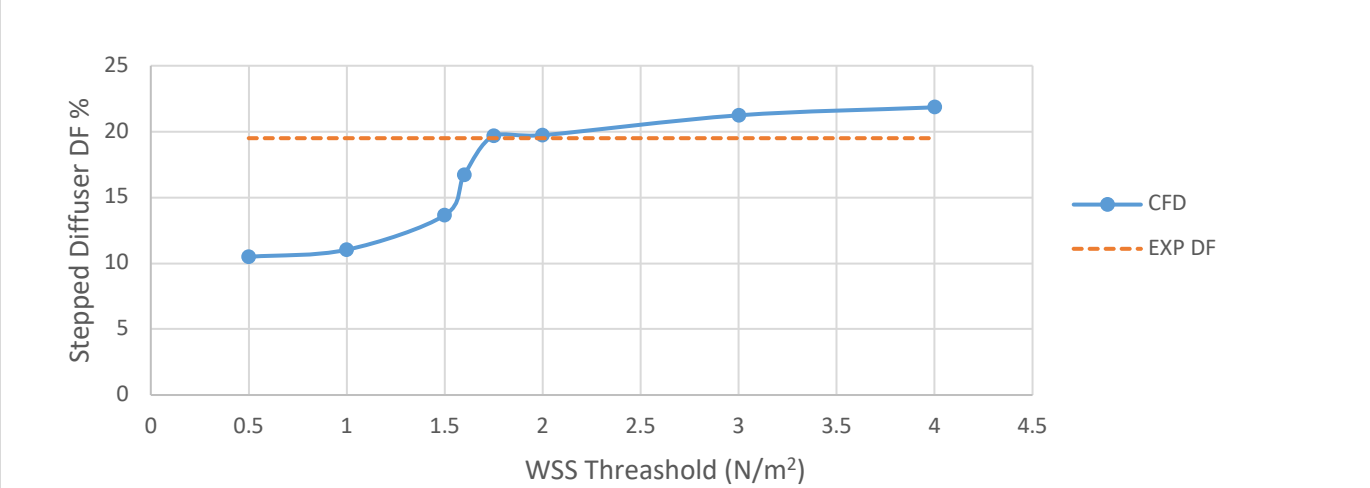

Figure 8: Deposition fraction in the stepped diffuser as a function of WSS Threshold

Effects of increasing flow rate

The effects of increasing flow rate for a full-term infant cannula were examined for the gradual diffuser and reported in Figure (9). As expected, particle losses increased as flow transitioned from its transitional nature at 2 L/min to turbulent at 5 L/min. However, this rate of increase slows down at high flow rates. It is likely that at some flow rate, DF will plateau. The increase in DF is associated with an increase in the jet strength and turbulent kinetic energy as shown in Figures (10-17).

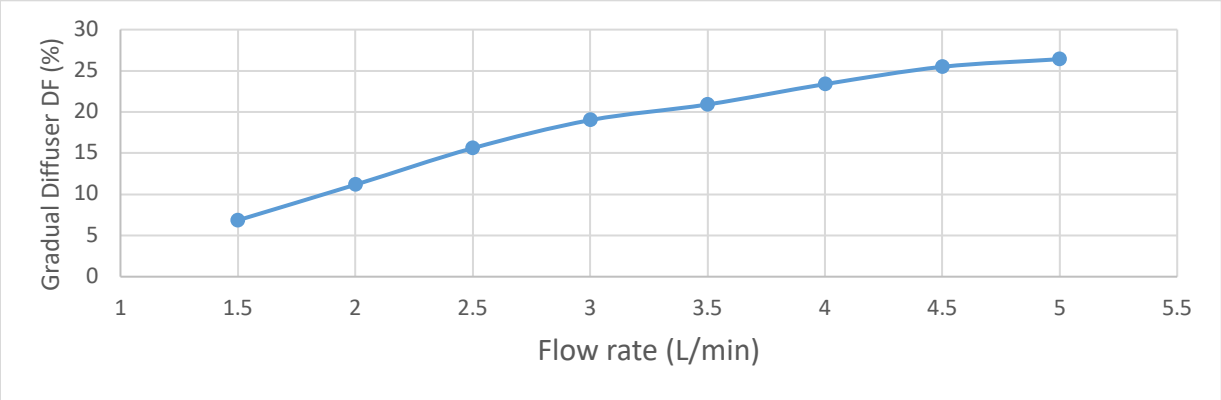

Figure 9: DF in the gradual diffuser as a function of flow rate

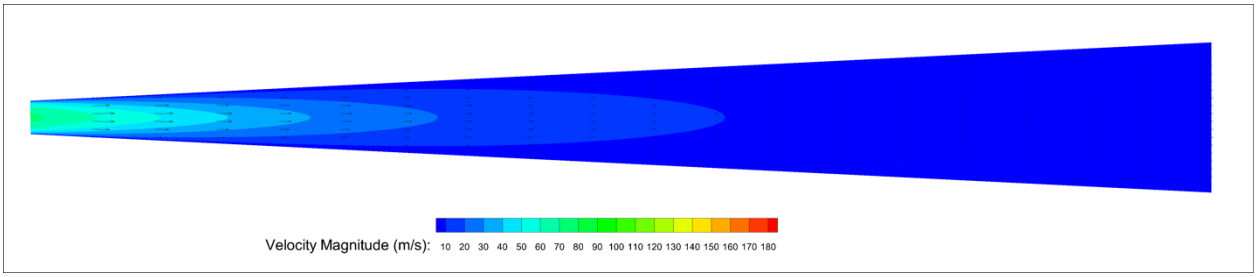

Figure 10: Velocity field in the gradual diffuser at 2 L/min

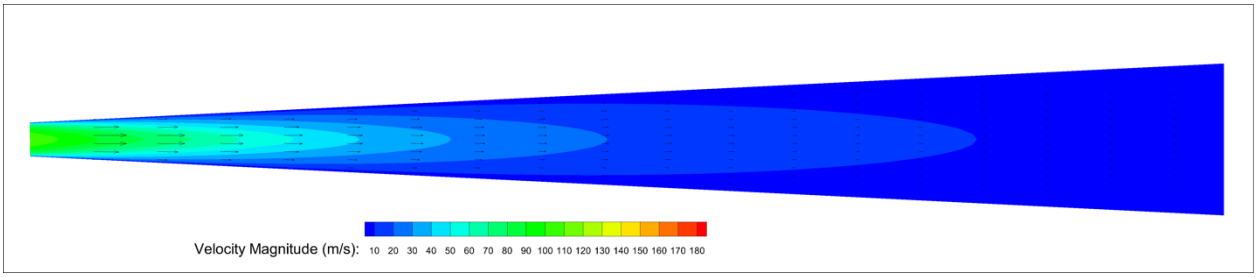

Figure 11: Velocity field in the gradual diffuser at 3 L/min

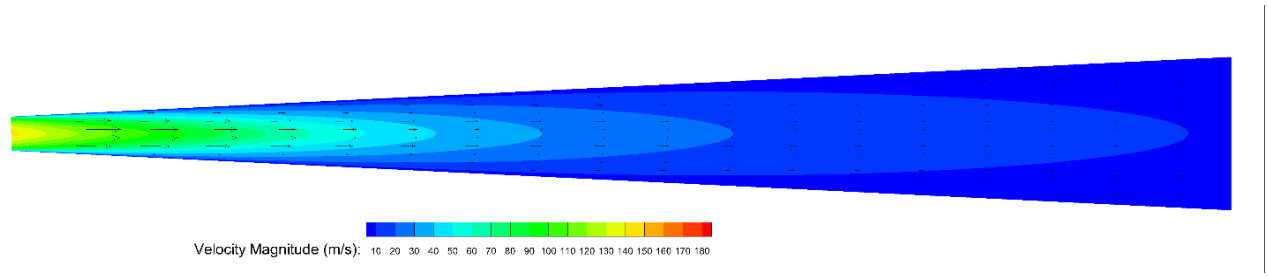

Figure 12: Velocity field in the gradual diffuser at 4 L/min

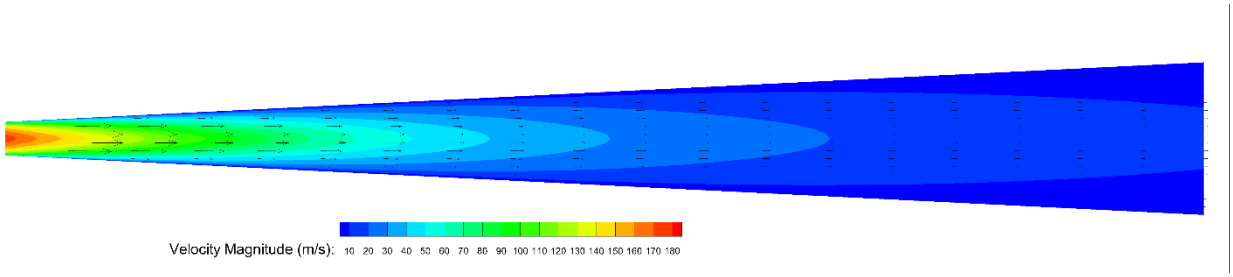

Figure 13: Velocity field in the gradual diffuser at 5 L/min

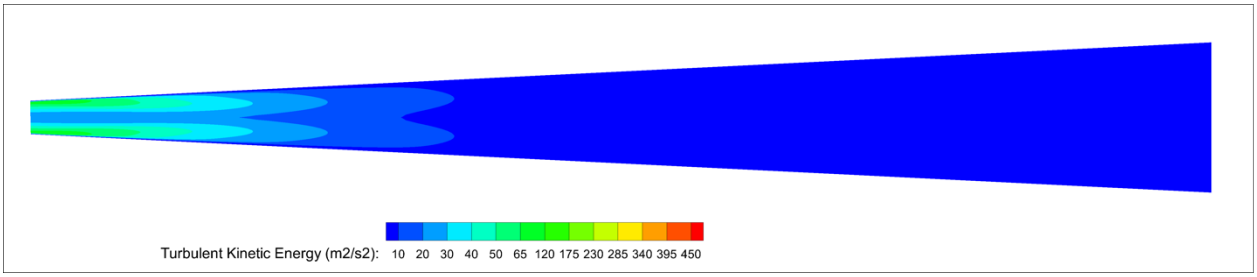

Figure 14: Turbulent kinetic energy in the gradual diffuser at 2 L/min

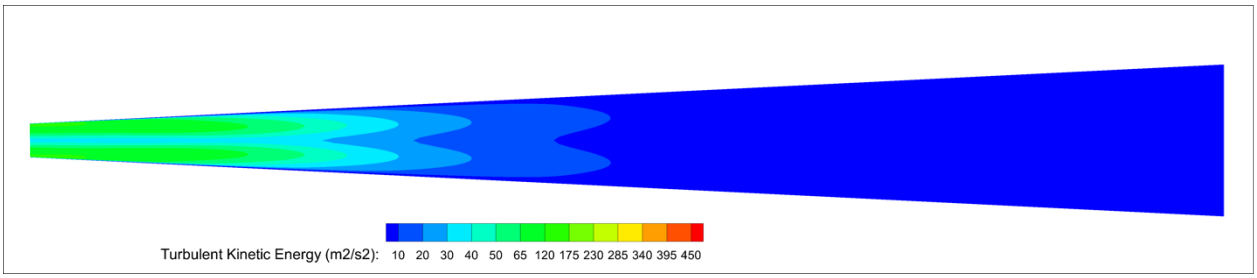

Figure 15: Turbulent kinetic energy in the gradual diffuser at 3 L/min

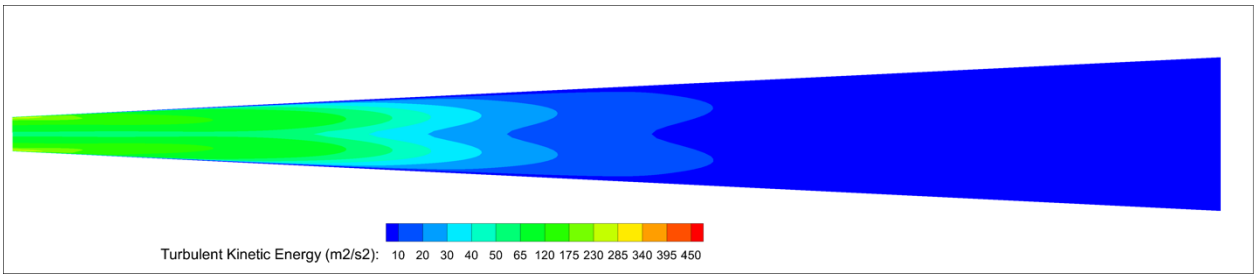

Figure 16: Turbulent kinetic energy in the gradual diffuser at 4 L/min

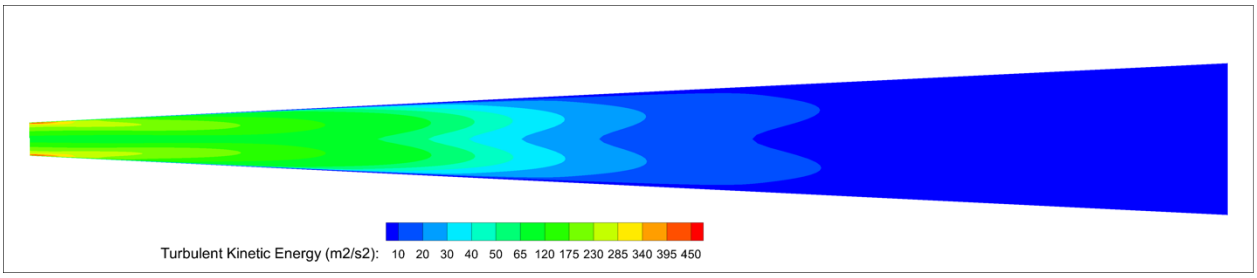

Figure 17: Turbulent kinetic energy in the gradual diffuser at 5 L/min

Effects of increasing wall roughness

The effects of increasing wall roughness are considered for the gradually expanding cannula. Figure (18) shows the effects varying wall roughness height on the skin friction coefficient, C_f. At 2 L/min, C_f is slightly changed. However, at 5 L/min, C_f increases 25 % as wall roughness is increased from 5 to 40 µm. The effect of increasing wall roughness on cannula DF were considered at various flow rates as shown in Figure (19). Interestingly, DF was found to decrease as the cannula surface became rougher regardless of the flow nature. DFs at all flow rates start to converge as walls become very rough.

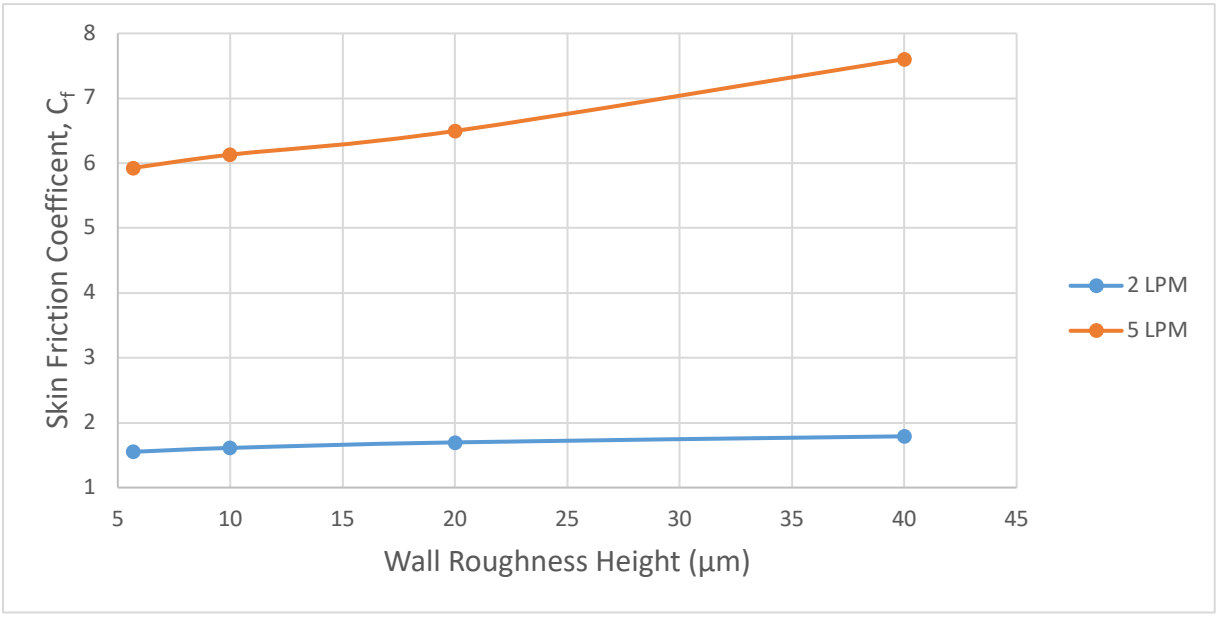

Figure 48: Skin Friction Coefficient as a function of the gradual diffuser wall roughness

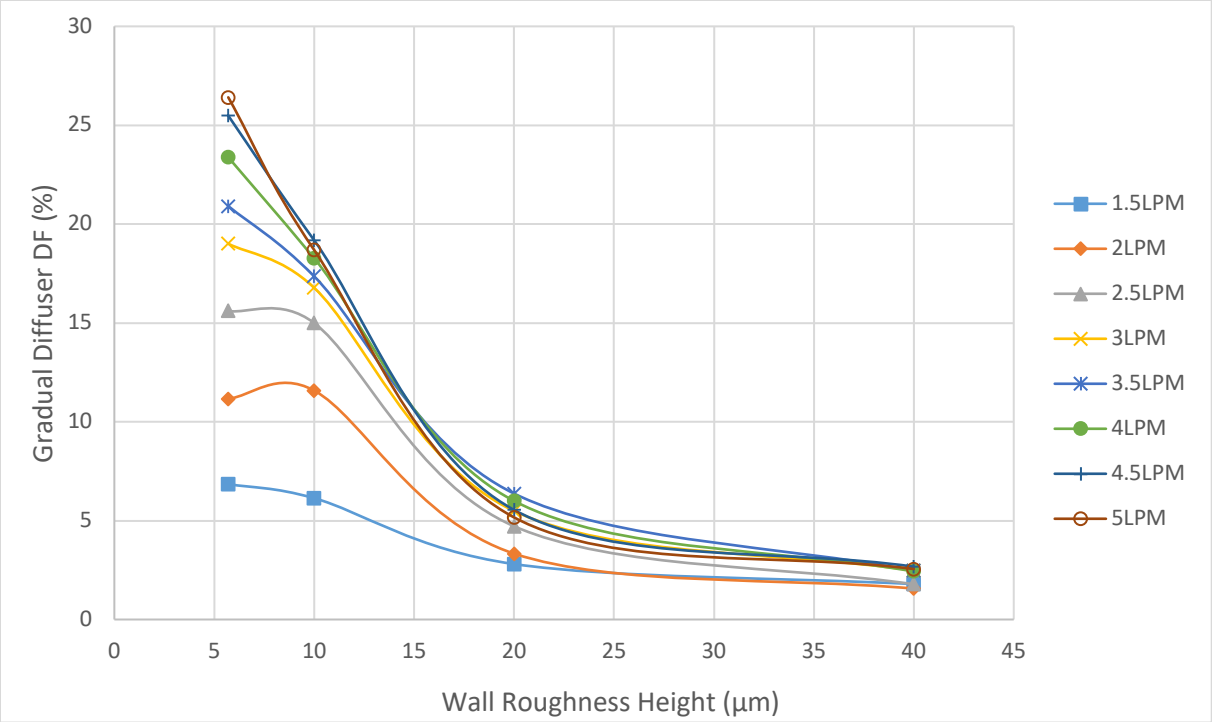

Figure 19: The effect of wall roughness and flow rate on aerosol losses

To isolate the role of WSS mechanism on DF from the effects of wall roughness, particle injections were repeated at 2, 3 and 5 L/min without using the particle reflection code. In this case, the reversed trend was observed; DF was found to increase when walls became rougher regardless of flow rate (Figure (20)). The implications of these observations will be discussed in the Chapter 6.

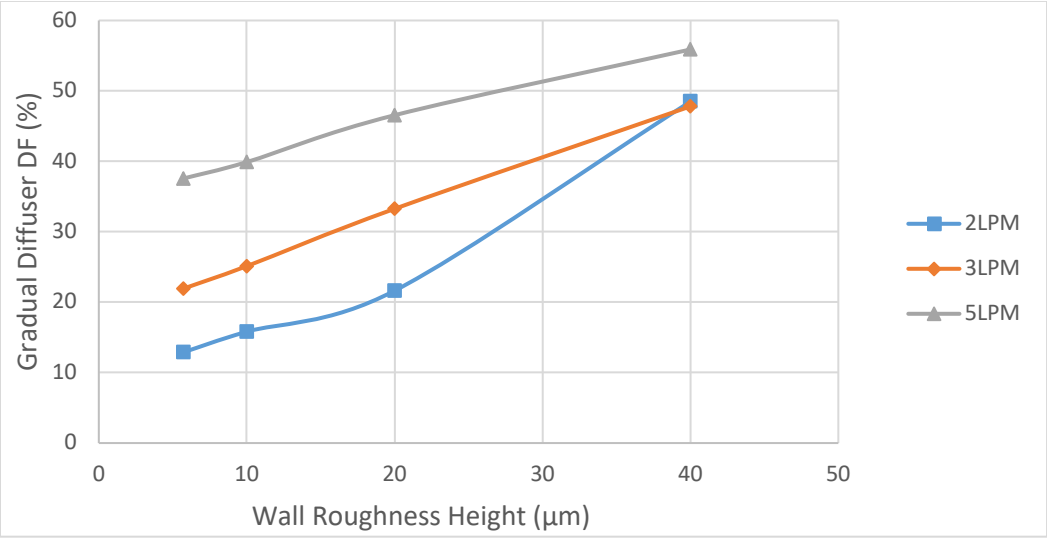

Figure 20: The effect of wall roughness and flow rate on aerosol loss without using the WSS code

Chapter 4

In this chapter, we consider several approaches to enhance the performance of the two-diffuser types. These approaches include streamlining the gradually expanding cannula and changing the lengths of the step and flat parts of stepped design. We also introduce a third type of diffuser that is similar to the gradually expanding cannula. However, in this design we expand the inlet diameter to allow for airflow around the central jet at a user specified flow rate; we refer to this design as the co-flow design. Its performance was examined *in-silico* using our established model at various flow rate ratios between the central and external boundary inlets.

Streamlining the gradually expanding cannula

The gradually expanding cannula was streamlined by slightly curving its surface near the inlet and outlet without changing its length. At 3 L/min, cumulative DF for both straight and streamlined cannulas are plotted in Figure (21). In the straight cannula, particles start to deposit past the first 9 mm. Streamlining the cannula reduces this onset to 3 mm. Comparing these to the DF profiles without using the particle reflection code shows that WSS significantly reduces DF for both types of diffusers. However, this reduction does not provide a net advantage to the streamlined cannula since total DF was only reduced by 1%.

Modifying the stepped design

The performance of the stepped design was inspected by varying the lengths of the step and flat surfaces. Case 1 refers to the experimentally validated case discussed in Chapter 2. In Case 2, the length of the step was reduced to 3 mm while the length of the of the flat surface was extended to 7 mm. In the third case, the step length was reduced to 1 mm while the length of the flat surface was extended to 9 mm. In order to maintain the overall cannula length unchanged, the angle of divergence was increased in each case.

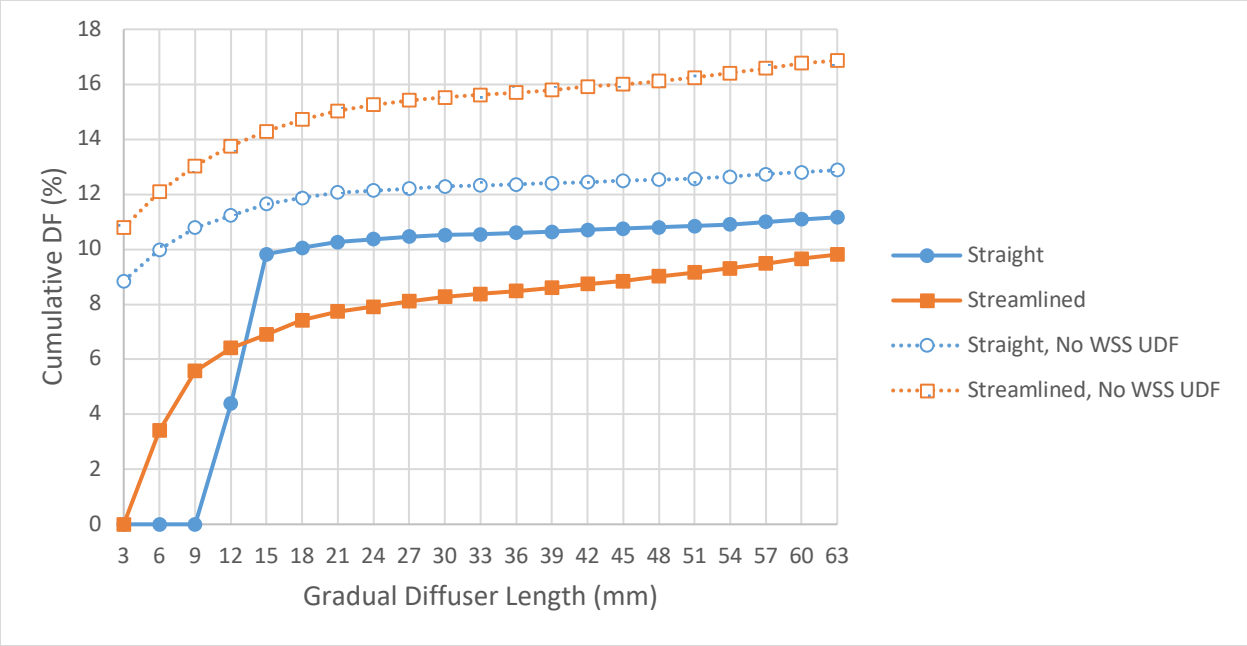

Figure 21: Cumulative DF in the gradual Diffuser

Figure (22) shows the total DF in each of the three cases. Moving from Case 1 to Case 3, cannula DF was found to increase regardless of the effect of the WSS mechanism.

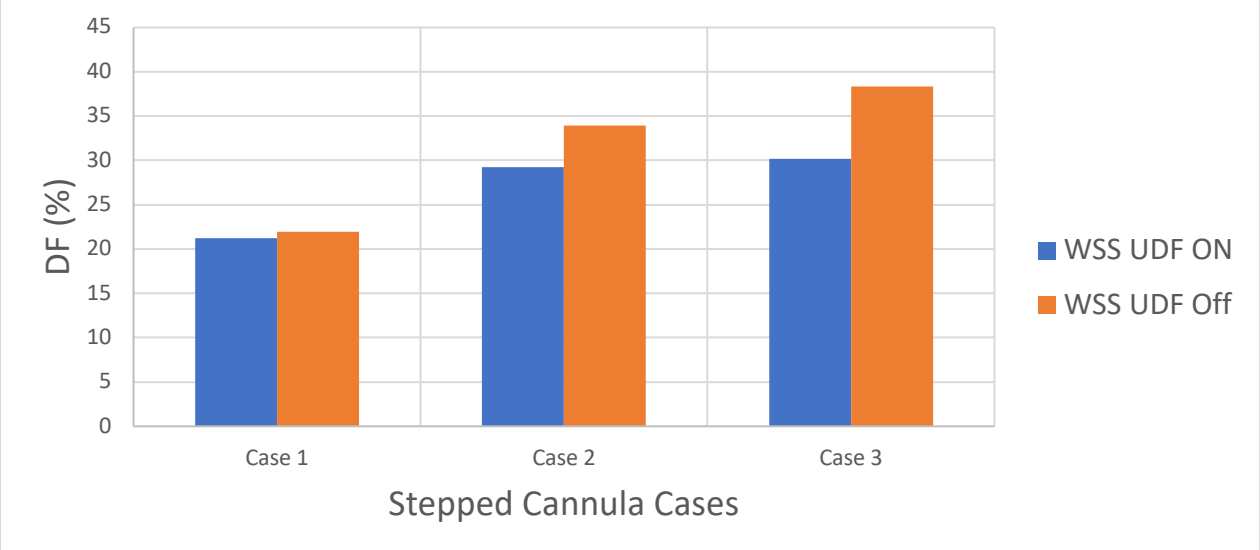

Figure 22: Deposition fractions in various modifications of the stepped cannula

Figures (23-25) show the flow field behavior across the mid-plane of each of the three geometries. In all three cases, flow recirculation, was found to occur. In Case 3, flow recirculation was strong enough that 2600 particles were trapped in these zones. Interestingly, the jet was found to attach to the upper surface in Case 2 only. This flow attachment was not part

of an oscillating behavior; as soon the simulation converged, flow remained attached to the surface.

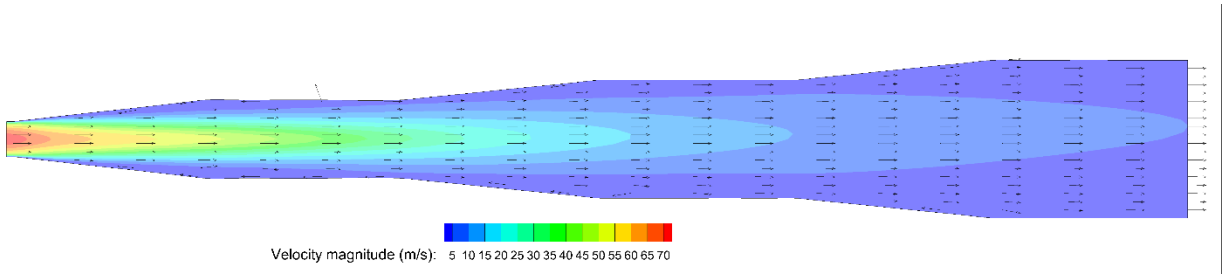

Figure 23: Flow field in stepped design, case 1

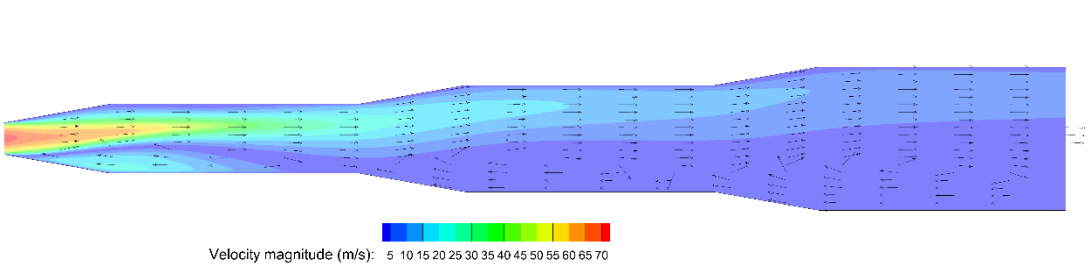

Figure 24: Flow field in a stepped design, case 2

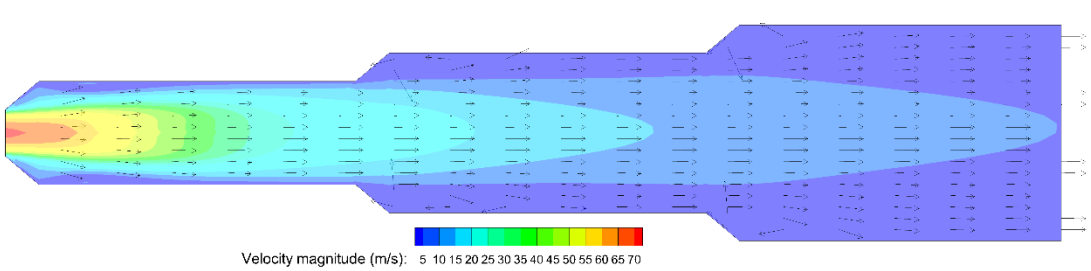

Figure 25: Flow field in stepped design, case 3

The co-flow design

Performance of the co-flow design was examined at 3 and 5 L/min. The ratio of external to central flow rate was varied from 50:50 to 20:80 in increments of 10 %. Figures (26) and (27) show the total DF in each of these cases at 3 and 5 L/min, respectively. At both flow rates, setting the co-flow inlet with a flow rate lower than that of central one increases DF even in the absence of the WSS mechanism.

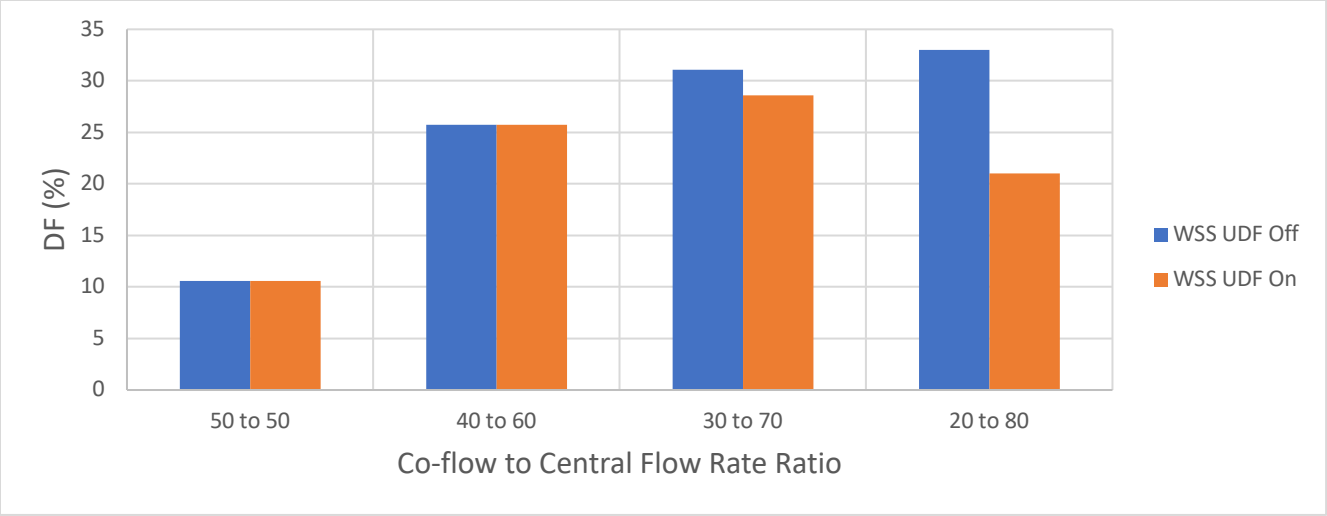

Figure 26: Deposition fractions in the co-flow diffuser at 3 L/min

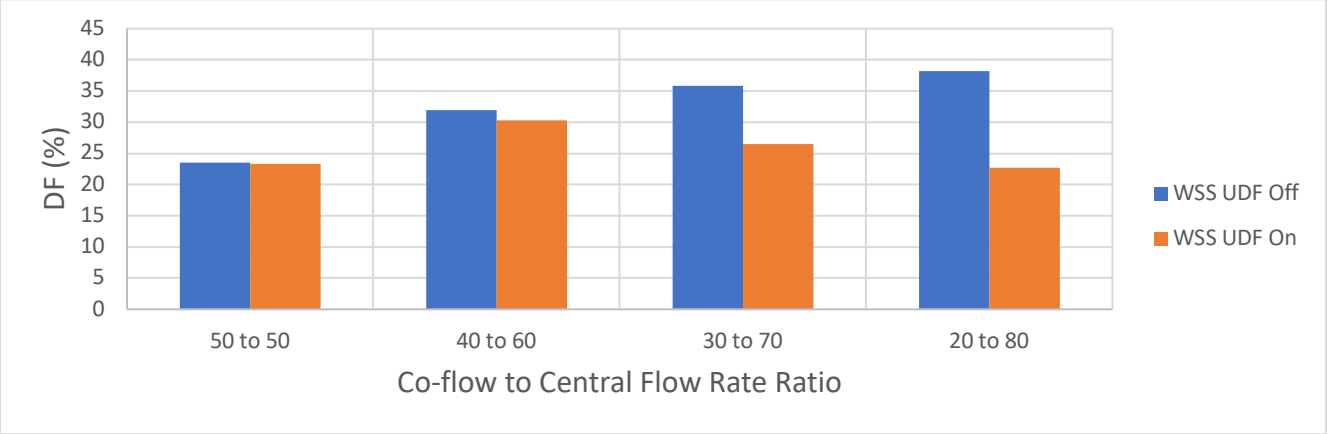

Figure 27: Deposition fractions in the co-flow diffuser at 5 L/min

Figures (28-31) show the flow behavior in the co-flow design for each of the four cases at 3 L/min. In these figures, vectors were intentionally drawn at uniform scale to highlight the presence of reversed flow. While no flow re-circulation was detected in the first two cases, it starts to occur when the percentage of central flow rate inlet is at least 70 %. Flow behavior was not examined for the four cases at 5 L/min.

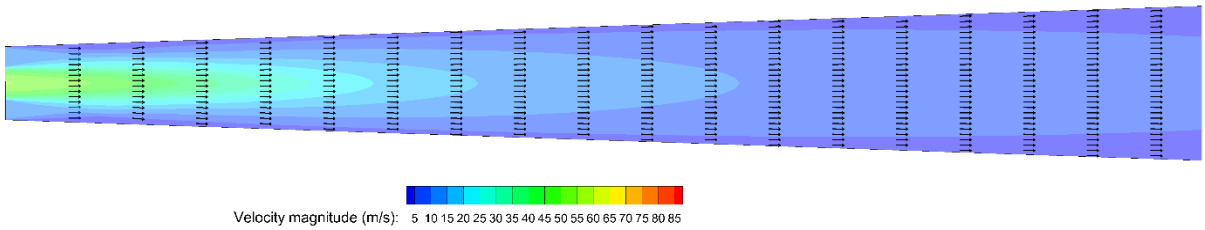

Figure 28: Flow behavior in a co-flow design with 50 % central flow rate.

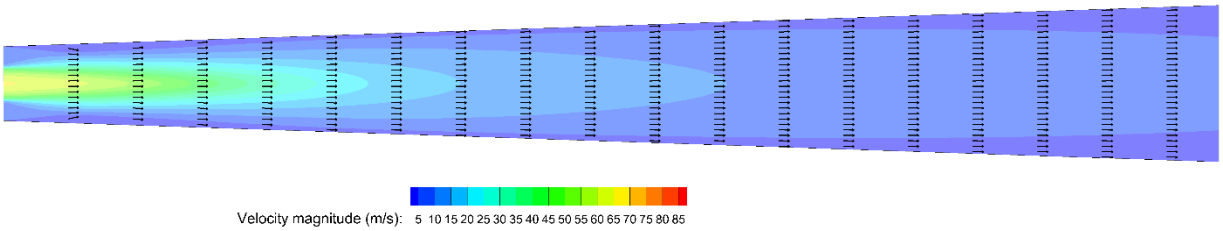

Figure 29: Flow behavior in a co-flow design with 60 % central flow rate.

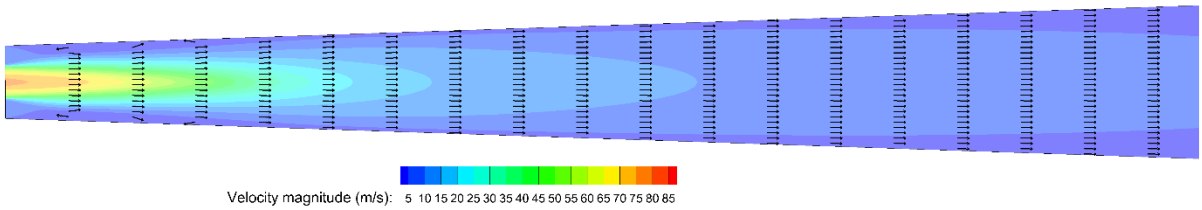

Figure 30: Flow behavior in a co-flow design with 70 % central flow rate.

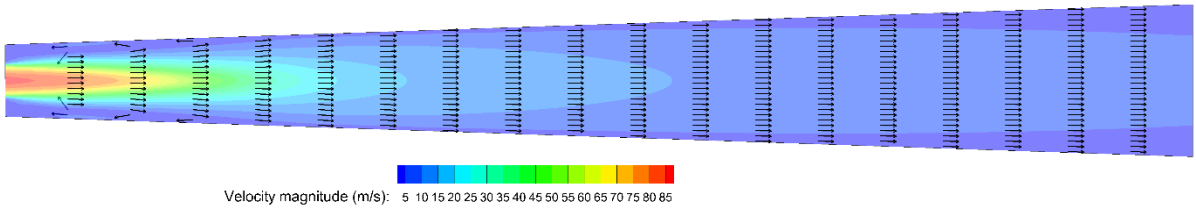

Figure 31: Flow behavior in a co-flow design with 80 % central flow rate.

Chapter 5

Optimizing the gradually expanding cannula

The 63 mm gradually expanding diffuser was extended to 70, 80, 90 and 100 mm. Flow simulations and particle injections were performed at 3 and 5 L/min for all designs. DFs in all cannulas are shown in Figure (32). At 3 L/min, extending the cannula from 70 mm to 100 mm successfully achieves the target DF (< 5 %). This reduction is primarily due to the additional WSS mechanism; when the particle reflection code was turned off, DF in any of the four designs was higher. However, in the absence of the additional mechanism, extending the cannula is still a DF reducing mechanism. This is likely due to the slight decrease in turbulent kinetic energy of the system at 3 L/min as shown in Figure (33).

Similarly, at 5 L/min, both turbulent kinetic energy and WSS mechanism play major roles in reducing particle losses. Figure (32) shows that DFs were higher in the absence of the WSS mechanism regardless of the cannula size. Figure (33) shows a decrease in volume averaged turbulent kinetic energy from 18 m^2/s^2 in a 70 mm cannula to 14 m^2/s^2 in a 100 mm cannula. However, extending the cannula above 90 mm reduces the effects of WSS on particle deposition, which, consequently, leads to an increase in DF. It is unknown whether this increase in deposition will continue if the cannula is further lengthened. However, the DF reached at 90 mm is very close to the target DF.

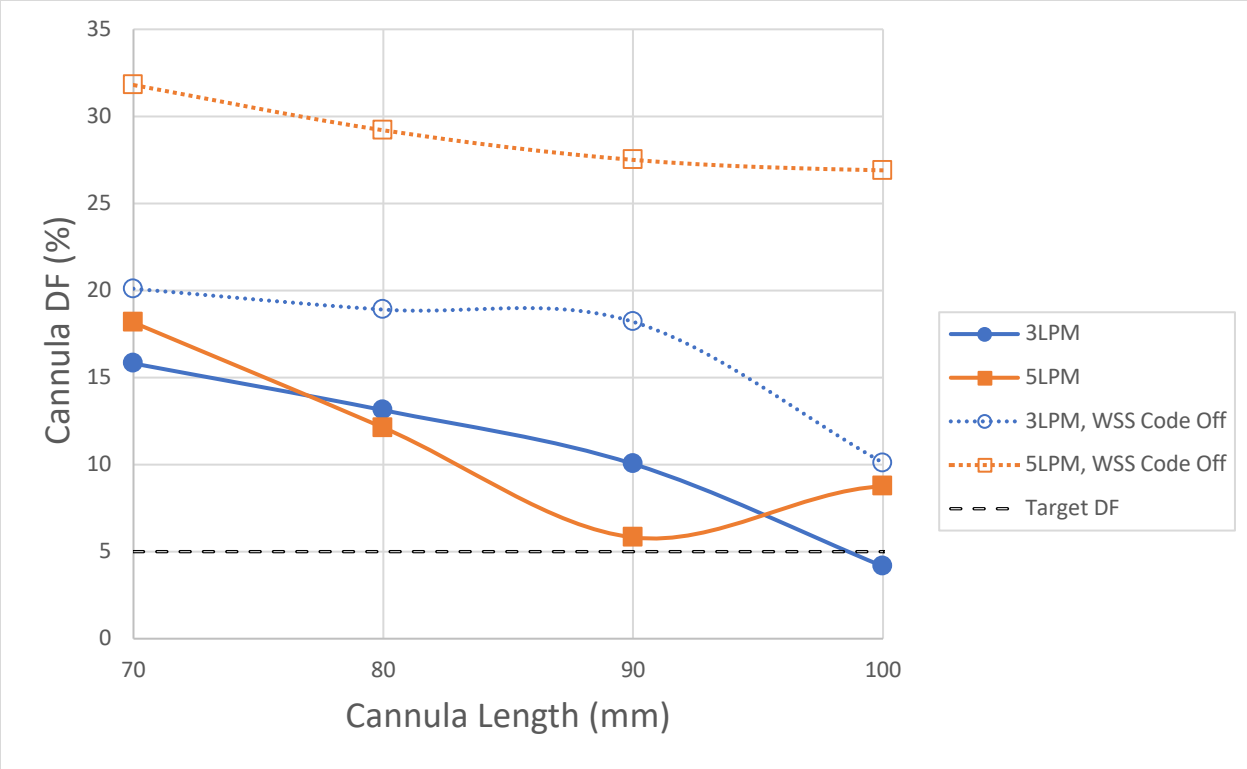

Figure 32: Deposition fractions in four modified gradual diffuser designs at 3 and 5 L/min.

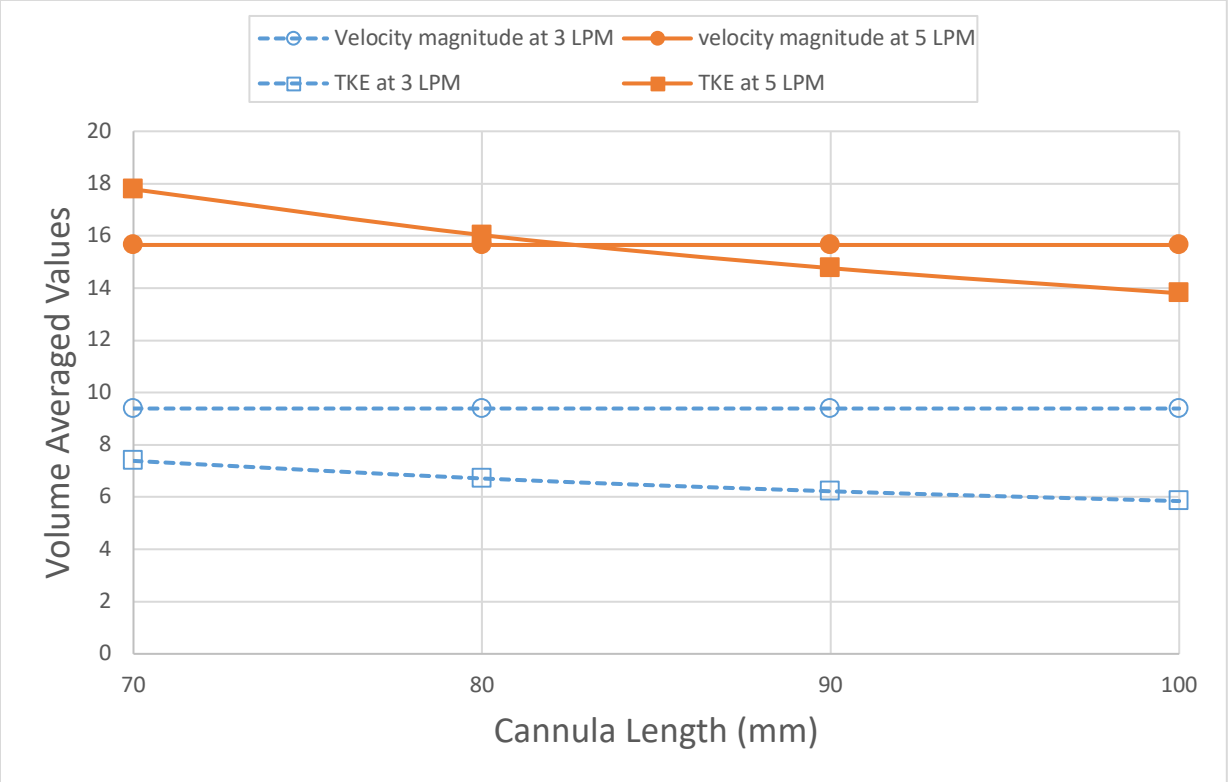

Figure 33: Volume averaged flow variables in the four modified gradual diffuser designs at 3 and 5 L/min

Optimizing the co-flow design

The co-flow design with equally distributed flow rates between the central and external inlets achieved the lowest DF among all co-flow designs. To further optimize its performance, this design was further extended to 70 mm, 80 m, and 90 mm. Deposition fractions in each of the three modified designs are plotted in Figure (34) at 3 and 5 L/min

In each of the three designs, WSS_{max} was found to be lower than the established WSS critical value. Thus, the particle reflection code had no effect on DFs in any of the six cases. The slight reduction in DF is likely due to the decrease of turbulence fluctuations. Figure (35) shows the variation of volume averaged flow field properties as the co-flow design is extended. At 3 L/min, minor decrease in DF is accompanied with minor decrease in turbulent kinetic energy. While at 5 L/min, a more severe decrease in DF was accompanied by steeper decrease in turbulent kinetic energy.

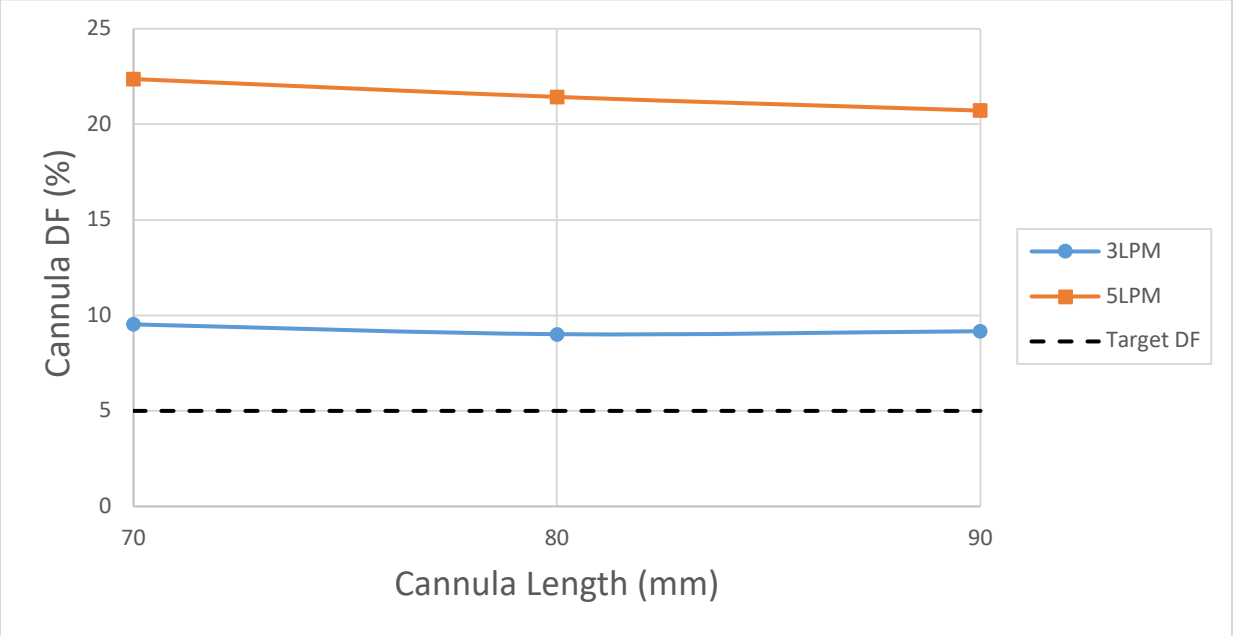

Figure 34: Deposition fractions in the three modified co-flow cannulas at 3 and 5 L/min

Since lengthening the co-flow diffuser provided no major advantage in minimizing aerosol losses, another approach was taken. Flow rates at the central and external inlets of the 70

mm design were adjusted based on velocity magnitude ratios. After adjusting the inlet boundary conditions, flow simulations and particle injections were again performed. DFs are plotted in Figures (36) and (37) at 3 and 5 L/min, respectively, and for various velocity ratios. In these figures, V1 and V2 correspond to the velocity magnitudes at the central and external inlets, respectively.

At both flow rates considered, reducing the ratio of V1 to V2 results in a continuous decrease in DF. Target DFs were achieved when the ratios of V1 to V2 were 2.90 and 1.70 at 3 and 5 L/min, respectively. The decrease in DF was accompanied by a decrease in turbulence. Figure (38) shows a decrease in turbulent kinetic energy as V1/V2 is reduced for a 5 L/min total flow rate. The effect of this change on particle depositions is shown in Figure (39). Since turbulence is more likely to affect small and medium size particles, the majority of the particles depositing when V1/V2= 0.7 have a diameter greater than 3µm.

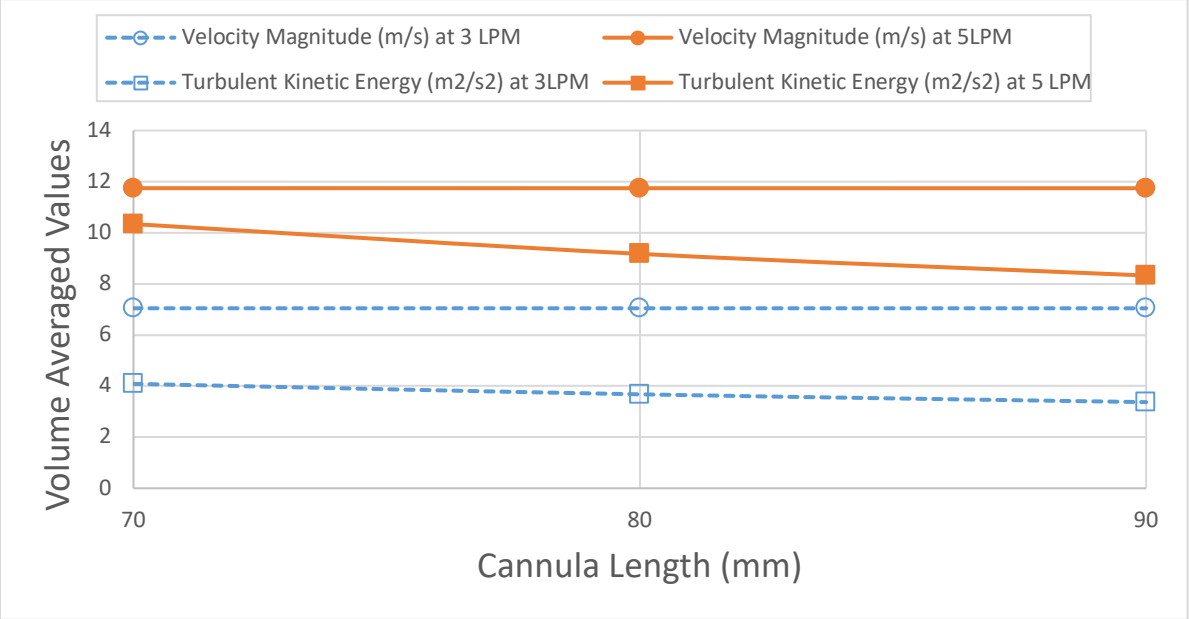

Figure 35: Volume averaged flow variables in the three co-flow design variations

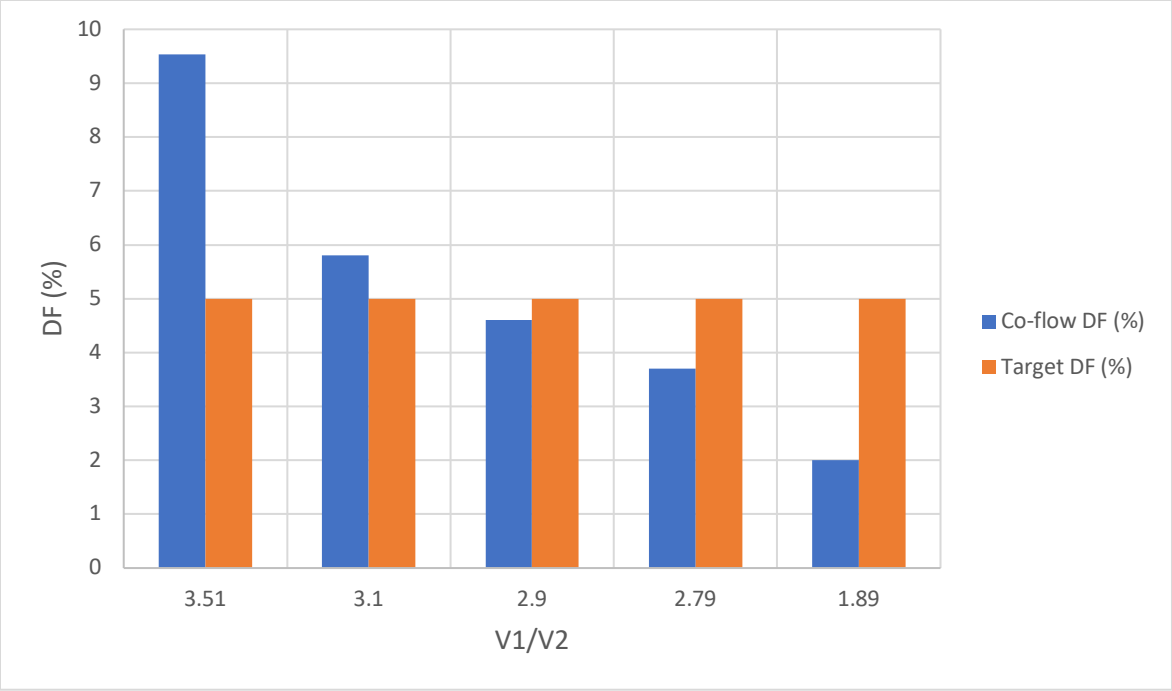

Figure 36: Deposition fraction in a 70 mm co-flow diffuser using various inlet velocity conditions at 3 L/min total flow rate.

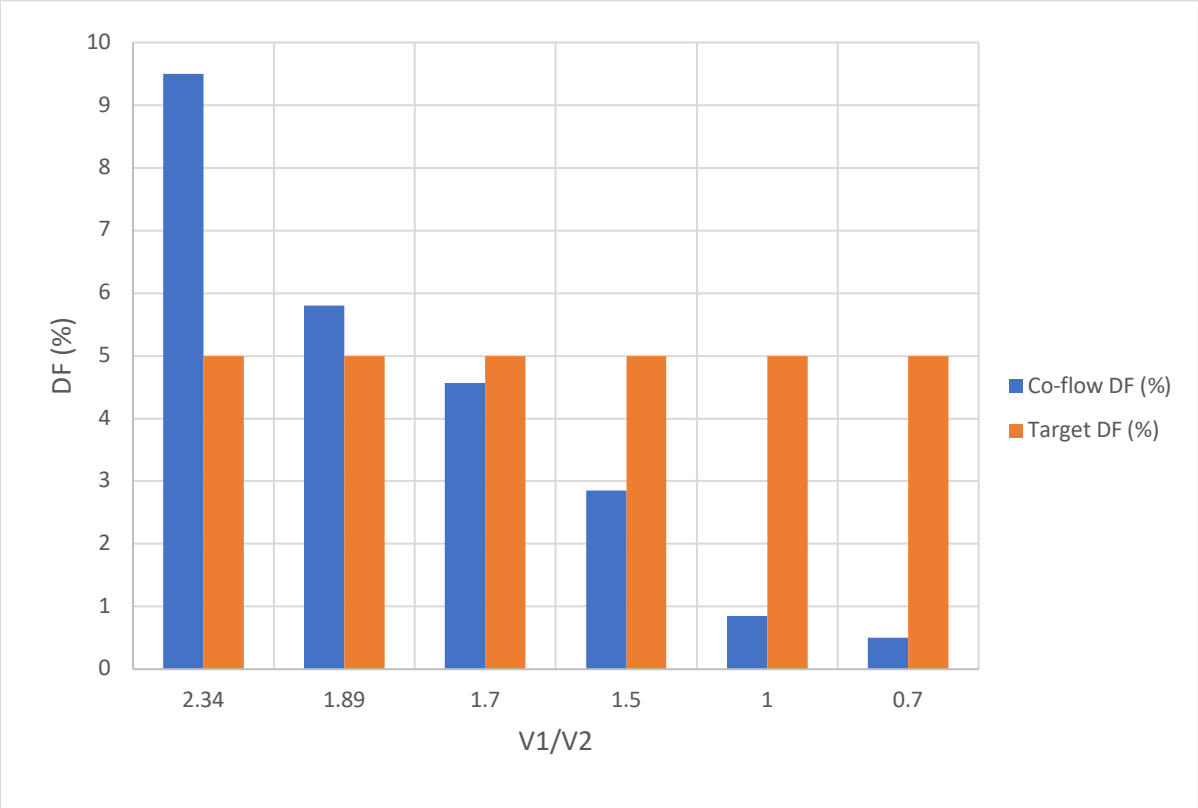

Figure 37: Deposition fraction in a 70 mm co-flow diffuser using various inlet velocity conditions at 5 L/min total flow rate.

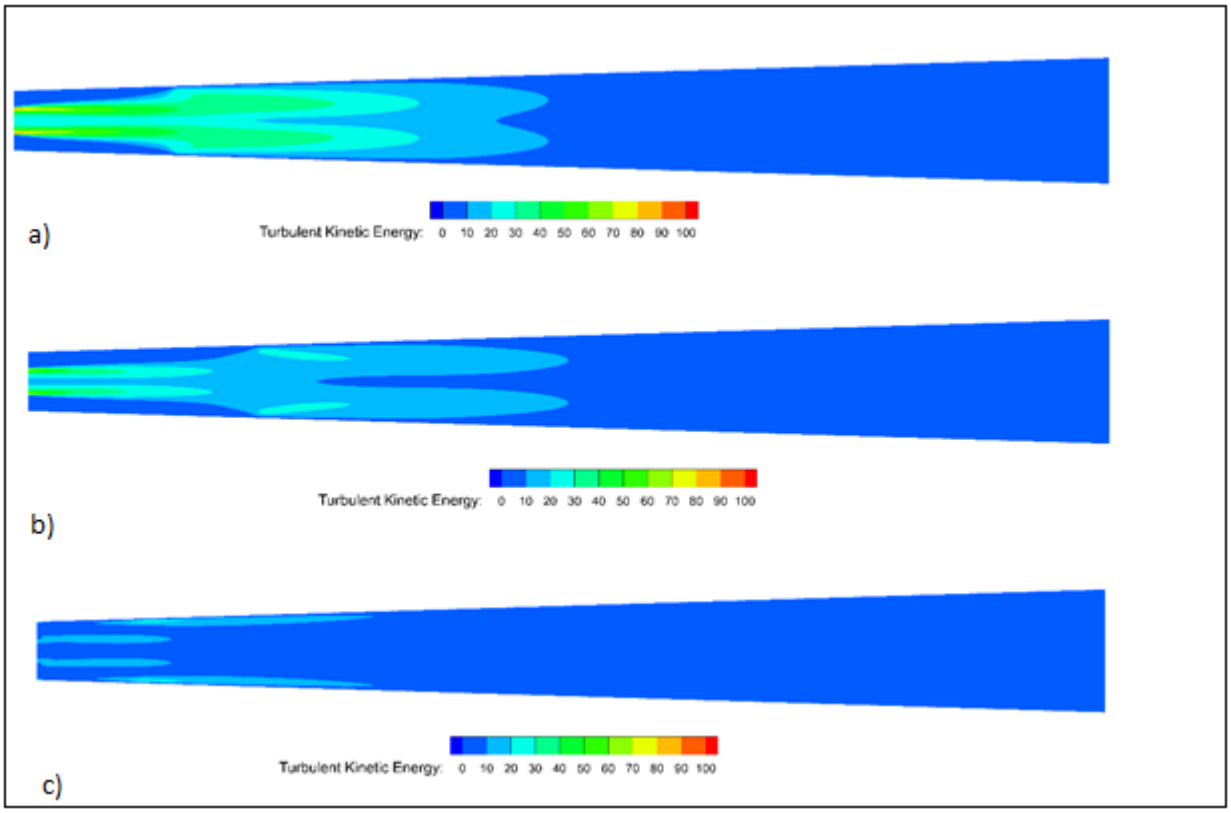

Figure 38: Turbulent kinetic energy contours in a 70 mm co-flow cannula midplane when a) V1/V2=2.34, b) V1/V2= 1.7, and c) V1/V2=0.7.

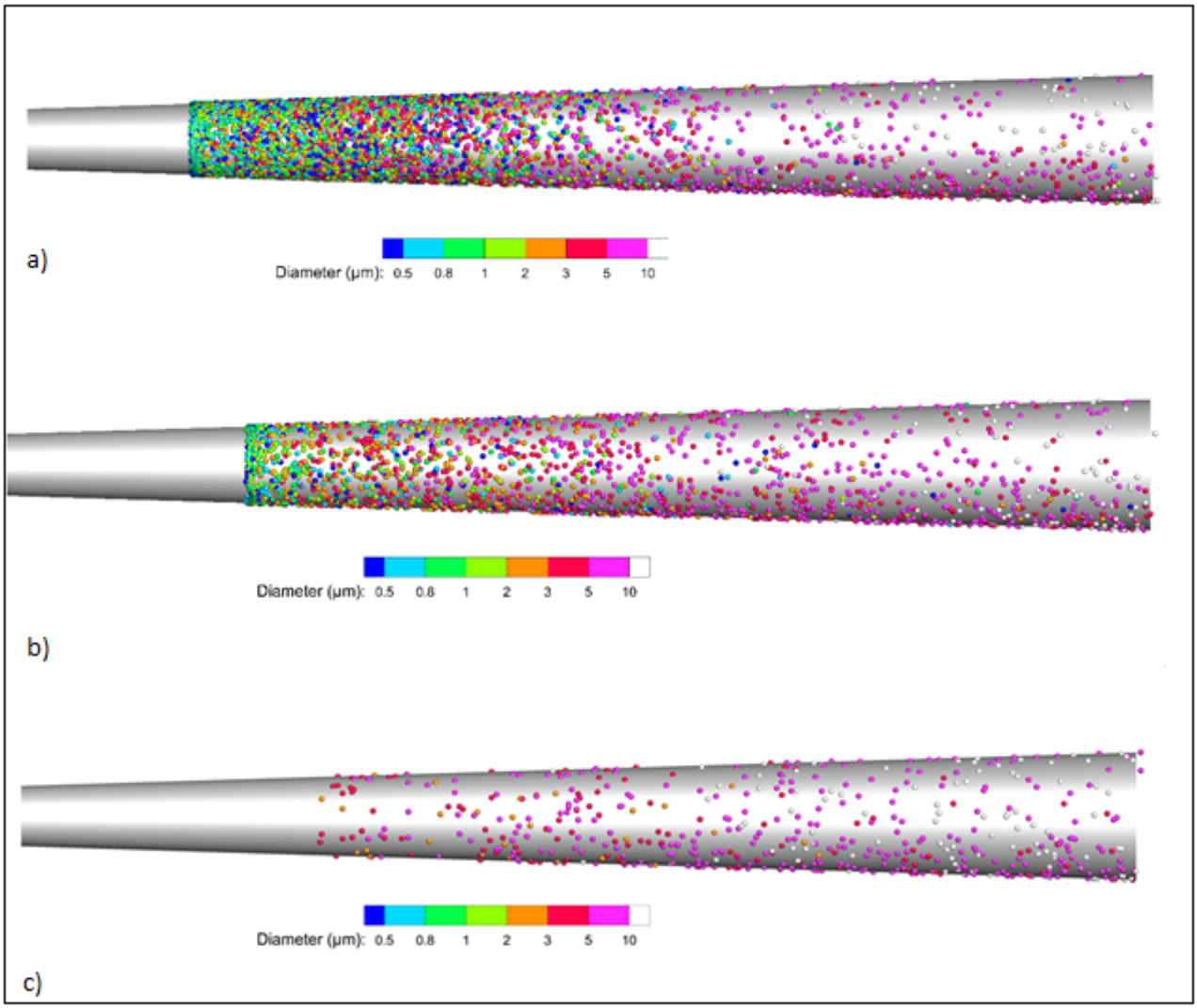

Figure 39: Particle deposition maps in a 70 mm co-flow cannula when a) V1/V2=2.34, b) V1/V2= 1.7, and c) V1/V2=0.7

Chapter 6: Discussion and Conclusion

In this study, turbulent kinetic energy and WSS were found to be primary factors in nasal cannula particle deposition. By lengthening the cannula designs and accounting for the effects of WSS on particle deposition, both gradual and co-flow designs were optimized to operate under the required conditions. 90 mm and 100 mm gradually expanding cannulas were predicted to achieve targeted delivery conditions at 3 L/min, and 5 L/min, respectively. A 70mm co-flow cannula also achieved the desired conditions by providing sheath airflow around the central jet.

The primary technical benefit that our CFD model offers is allowing particles to reflect based on the value of a flow field variable. While *Fluent* built-in *Discrete Phase Model* (DPM) has a boundary condition that permits particle reflection, this reflection cannot be conditional and could only be applied to the entirety of the flow field. In our code, the reflection condition could be set to any wall-related property. The algorithm of the code was validated by comparing deposition fraction in two cases. In the first case, the particle reflection condition was set to occur until some point along the stream-wise direction of the cannula is reached. In the second case, the same cannula design was perpendicularly split into two portions at the same point coordinates from the first case. The *DPM* reflection boundary condition was set to reflect all particles that impact the portion closer to the cannula inlet and trap all particles that impact within the other portion. Both cases resulted in the same DF confirming that the algorithm of the code is correct.

While turbulence is a perceived as a beneficial particle dispersion mechanism, it is also a major source of particle loss. Increasing flow rate of the base gradual diffuser from 2 L/min to 5 L/min resulted in more than a 2-fold increase in DF due to the rise in turbulent kinetic energy. Thus, a key factor in reducing drug depositional loss in the cannula is turbulent kinetic energy.

Extending the length of a cannula was found to be a good approach in reducing turbulence fluctuations.

In this work, streamlining the cannula interface was not found to be very advantageous. In contrary to our findings, studies done by VCU labs [13] [14] demonstrated that streamlining the nasal cannula reduces drug losses significantly. This discrepancy is likely because their streamlining approach targeted sharp turns within the cannula which was not the case in this work. That is, in this study, streamlining flow angles of approximately 175-degrees had little impact.

Our results indicate that surface roughness is a sensitive parameter in the CFD model. In a study previously done by our lab, Holbrook et al. [10] evaluated the effects of surface roughness on the local deposition of micrometer particles in an *in-vitro* asymmetric double bifurcation geometry. The degree of surface roughness selected in the CFD sub-model had minor effect on deposition. The authors attributed this to the laminar nature of the flow and predicted a greater role of surface roughness in a turbulent flow regime. Our results are in qualitative agreement with Holbrook et al. [10] findings. In the presence of a WSS mechanism, the variations in DF were significantly wider at 5 L/min than those at 1.5 L/min.

Cannulas utilized *in-vitro* were printed using a glossy resin-plastic material that had 5.7 μm roughness. However, if printed using a different material, wall roughness measurements will vary. The roughness study discussed in Chapter 2 can support experimentalists in gaining insight on effect that different materials could have on the particle deposition.

In turbulent flow, the correlation between wall roughness and particle deposition is quite complex. In the absence of the additional WSS mechanism, more particles deposited as friction coefficient is increased. However, in the presence of the WSS mechanism, DF was reduced as

walls became rougher. This suggests that the effects of friction, predicted by *Fluent*, were in contrast with the additional WSS mechanism. One possible explanation is that the UDF does not re-integrate the corrected values of WSS into the numerical model. Nonetheless, it is possible that the additional mechanism provides physical insight that was initially not captured by the CFD model; rough walls can cause an increase turbulent fluctuations and wall shear stress values which could result in more particles stripping from the cannula surface.

Boundary layer separation is common phenomenon that occurs in various flow regimes including flow in a conical diffuser [15]. The onset of boundary layer de-attachment is dependent the divergence angle, length to diameter (L/D) ratio, and inlet turbulence[16-18]. Our primary motivation behind extending all diffuser designs was to detect and, possibly, delay boundary layer separation. For the gradual and co-flow diffusers, we considered angle variations between 2-4° and L/D ratio between 70 and123. Turbulence intensity was only changed according to flow rate. Nonetheless, flow separation was not detected in any of the two design types. The literature is rich with studies concerning critical values of angles and L/D ratios, however, large L/D ratios (> 65) are rarely discussed for conical diffusers.

For the stepped diffuser, it is likely that a shorter step can delay the onset the of flow separation. However, recirculation regions were observed in all stepped diffusers. This shows that the increase in the angle of divergence had a stronger influence on flow separation than step length. Flow attachment to the upper surface that occurred in Case 2 of the modified stepped design was a result of the low-pressure vortex that pushed the jet to the other side of the cannula. The phenomenon -referred to as the *Coanda effect*- was absent in other two cases which suggests a more complex mechanism between flow attachment and diffuser design that was not examined in this study. Strong recirculation regions as those encountered in the stepped diffuser are likely

to present a computational challenge as particles that are entrapped within these regions may not have a definitive fate. This can lead to high standard deviations when estimating deposition fractions. For this reason and the lack of understanding of flow attachment/ de-attachment in these designs, the stepped diffuser was not considered in the optimization stage.

While the study performed has promising results, it suffers from several limitations. The implemented UDF assumes that the critical WSS condition at which particles start to reflect is the same for all cases considered. This assumption needs to be further examined numerically and experimentally. For preterm infants, the optimized co-flow design is less likely to be practical option. Since the flow rate requirement is much smaller, a large fraction of the flow rate will need to be delivered through the capillary to achieve particle dispersion. Further understanding of boundary layer de-attachment is necessary for the stepped diffuser to be optimized.

Developing and optimizing cannula designs for improved aerosol delivery by the nose-to-lung route has a vast scope and is an active area of research. It has been found that incorporating 3D rod arrays leads to more efficient drug delivery due to reduced velocities and damped turbulent kinetic energy [4] . In the future, we would like to design and test cannulas with 3D rod arrays for a more efficient drug delivery. Observations from the study such as the wall roughness effects are already being considered for a follow-up of this work.

Another major area of research to achieve high efficiency lung delivery of aerosols is through using excipient enhanced growth (EEG) approach. In EEG, drug particles are initially in the primary sub-micrometer range that contain the surfactants and a hygroscopic excipient. The initial small size of the aerosolized particles allows for effective penetration through the nasal delivery system, such as the cannulas, and infant upper airways. Inclusion of the hygroscopic excipient in the primary particles fosters aerosol size increase inside the lungs due to increased

humidity and enables effective deposition in the targeted alveolar region. Integrating efficient cannulas, EEG approach, and 3D rod into a new non-invasive high efficiency lung delivery system is the foreseen future work.

References:

1. Longest, P.W., L. Golshahi, and M. Hindle, *Improving pharmaceutical aerosol delivery during noninvasive ventilation: Effects of streamlined components.* Annals of Biomedical Engineering, 2013. **41**(6): p. 1217-1232.

2. Golshahi, L., et al., *The use of condensational growth methods for efficient drug delivery to the lungs during noninvasive ventilation high flow therapy.* Pharmaceutical Research, 2013. **30**: p. 2917-2930.

3. Holbrook, L.T. and P.W. Longest, *Validating CFD predictions of highly localized aerosol deposition in airway models: In vitro data and effects of surface properties.* Journal of Aerosol Science, 2013. **59**: p. 6-21.

4. White, F.M., *Fluid mechanics.* 2015.

5. Fox, R.W. and S. Kline, *Flow regimes in curved subsonic diffusers.* Journal of Basic Engineering, 1962. **84**(3): p. 303-312.

6. Moore Jr, C.A. and S.J. Kline, *Some effects of vanes and of turbulence in two-dimensional wide-angle subsonic diffusers.* 1958.

7. McDonald, A.T. and R.W. Fox, *Incompressible Flow in Conical Diffusers*. 1964, PURDUE RESEARCH FOUNDATION LAFAYETTE IN LAFAYETTE United States.

8. Longest, P.W., et al., *Aerodynamic factors responsible for the deaggregation of carrier-free drug powders to form micrometer and submicrometer aerosols.* Pharmaceutical Research, 2013. **30**: p. 1608-1627.